Stockholm University

Modelling Organometallic Catalysis and Reactions in Cavitands

Joannes Peters

Doctoral Thesis in Organic Chemistry at Stockholm University, Sweden 2025

Modelling Organometallic Catalysis and Reactions in Cavitands

Joannes Peters

Academic dissertation for the Degree of Doctor of Philosophy in Organic Chemistry at Stockholm University to be publicly defended on Friday 2 May 2025 at 14.00 in Magnéli Hall, Arrhenius Laboratory, Svante Arrhenius väg 12D.

Abstract

Computational chemistry addresses chemical problems by modelling chemical processes through calculations, and has proven to be an excellent tool for conducting chemical research. This thesis focuses on the modelling of chemical reactions using density functional theory. These chemical reactions are divided into two categories: two reaction mechanisms in organometallic catalysis, and three different binding and/or mechanistic studies involving supramolecular cavitands. The calculations uncover mechanistic details and origins of selectivity which experiments alone could not have explained.

The first organometallic reaction studied concerns the dehydrogenation of amines with (cyclopentadienone)iron carbonyl. The results show a stepwise mechanism involving a rate-limiting hydride transfer followed by a much faster proton transfer. The calculations contribute to a more nuanced understanding of the reaction mechanism in general. The second reaction studied is the gold-catalysed cycloisomerisation of acetylenic acids to lactones. A detailed mechanism of the cycloisomerisation reaction was calculated, and the origins of the observed regioselectivity and stereoselectivity were uncovered. The results show a strong favouring of a mechanism involving an *anti*-addition of the carboxylic acid to the alkyne moiety, yielding (*Z*)-*exo*-alkylidene γ-lactones in the case of substituted alkynes.

The first reaction in a supramolecular cavitand considered here is the aforementioned cycloisomerisation of acetylenic acids, this time in a gold-functionalised resorcin[4]arene-based cavitand. The calculations give insights into the structure-activity relationship between the cavitand and several substituted alkyne-acids. Furthermore, the calculations show that the cavitand itself has a modest catalytic power. A binding study of several hydrophilic molecules in a resorcin[4]arene-based cavitand with pyridinyl-benzimidazole panels was conducted. It was found that the water molecules form a hydrogen-bonding network between the panels of the cavitand, as well as on the hydrophilic rim. These interactions explain the high binding affinity of hydrophilic molecules to a hydrophobic cavitand. Finally, the mechanism for the hydrolysis of acetylcholine in a similar resorcin[4]arene-based cavitand was investigated to discern possible catalytic applications. The calculations show that the hydrolysis reaction is associated with prohibitively high barriers inside of the cavitand, and hence the cavitand cannot catalyse this reaction.

Keywords: *computational chemistry, organometallic catalysis, supramolecular chemistry, cavitand, gold.*

Stockholm 2025
http://urn.kb.se/resolve?urn=urn:nbn:se:su:diva-240992

ISBN 978-91-8107-168-9
ISBN 978-91-8107-169-6

Department of Chemistry

Stockholm University, 106 91 Stockholm

MODELLING ORGANOMETALLIC CATALYSIS AND REACTIONS IN CAVITANDS

Joannes Peters

Stockholm
University

Modelling Organometallic Catalysis and Reactions in Cavitands

Joannes Peters

ISBN print 978-91-8107-168-9
ISBN PDF 978-91-8107-169-6

Printed in Sweden by Universitetsservice US-AB, Stockholm 2024

Strong steel is forged by melting weak iron, and true glory is forged through perseverance in the face of hardship. Anything free of cost is equally devoid of value.

Abstract

Computational chemistry addresses chemical problems by modelling chemical processes through calculations, and has proven to be an excellent tool for conducting chemical research. This thesis focuses on the modelling of chemical reactions using density functional theory. These chemical reactions are divided into two categories: two reaction mechanisms in organometallic catalysis, and three different binding and/or mechanistic studies involving supramolecular cavitands. The calculations uncover mechanistic details and origins of selectivity which experiments alone could not have explained.

The first organometallic reaction studied concerns the dehydrogenation of amines with (cyclopentadienone)iron carbonyl. The results show a stepwise mechanism involving a rate-limiting hydride transfer followed by a much faster proton transfer. The calculations contribute to a more nuanced understanding of the reaction mechanism in general. The second reaction studied is the gold-catalysed cycloisomerisation of acetylenic acids to lactones. A detailed mechanism of the cycloisomerisation reaction was calculated, and the origins of the observed regioselectivity and stereoselectivity were uncovered. The results show a strong favouring of a mechanism involving an *anti*-addition of the carboxylic acid to the alkyne moiety, yielding (*Z*)-*exo*-alkylidene γ-lactones in the case of substituted alkynes.

The first reaction in a supramolecular cavitand considered here is the aforementioned cycloisomerisation of acetylenic acids, this time in a gold-functionalised resorcin[4]arene-based cavitand. The calculations give insights into the structure-activity relationship between the cavitand and several substituted alkyne-acids. Furthermore, the calculations show that the cavitand itself has a modest catalytic power. A binding study of several hydrophilic molecules in a resorcin[4]arene-based cavitand with pyridinyl-benzimidazole panels was conducted. It was found that the water molecules form a hydrogen-bonding network between the panels of the cavitand, as well as on the hydrophilic rim. These interactions explain the high binding affinity of hydrophilic molecules to a hydrophobic cavitand. Finally, the mechanism for the hydrolysis of acetylcholine in a similar resorcin[4]arene-based cavitand was investigated to discern possible catalytic applications. The calculations show that the hydrolysis reaction is associated with prohibitively high barriers inside of the cavitand, and hence the cavitand cannot catalyse this reaction.

Populärvetenskaplig sammanfattning

Kemi finns överallt omkring oss – och inte bara i stora kemiska fabriker eller laboratorier. Den finns där när du tar medicin, när du dricker renat vatten från din kran, när du läser just denna mening – och när din hjärna bearbetar orden du precis har läst.

Kemister i laboratoriet vet exakt vilka kemikalier de börjar med och kan ta reda på exakt vad de har i slutet. Men vad de inte kan veta med säkerhet är vad som händer däremellan. Och det är just här som många viktiga frågor inom kemin uppstår. Hur förändrades dessa kemikalier för att bli det man hittar i slutändan? Och om något oväntat sker, vilken del av denna omvandling orsakade det?

För att besvara dessa frågor kan vi använda beräkningsmetoder som simulerar kemiska reaktioner steg för steg. Dessa simuleringar kan ge detaljerade svar på hur snabbt reaktioner sker, vilka möjliga utfall som finns och till och med vilka som är sannolika eller omöjliga.

Här använder vi täthetsfunktionalteori (DFT) en mycket väletablerad beräkningsmetod, för att besvara de ovan nämnda frågorna för ett antal kemiska reaktioner. Dessa reaktioner kan delas in i två grupper. Den första är organometallisk katalys, där metallhaltiga föreningar påskyndar kemiska reaktioner som annars skulle ske mycket ineffektivt, om alls. Den andra gruppen handlar om supramolekylär kemi, där behållarformade molekyler, så kallade kavitander, fångar in andra molekyler och leder till unika beteenden som inte observeras i lösning.

Beräkningarna för de metallorganiska reaktionerna ger insikt i hur en järnkatalyserad reaktion går till och besvarar frågan om varför en reaktion med guld leder till en mycket specifik produkt. Samma reaktion med guld kan också utföras i en kavitand, och vi visar hur detta sker. Slutligen undersöker vi vad mer dessa kavitander kan göra – såsom att binda molekyler som egentligen inte borde kunna binda till dem och om de kan katalysera en reaktion som normalt kräver ett enzym.

Populairwetenschappelijke samenvatting

Scheikunde is overal om ons heen – en niet alleen in grote chemische fabrieken of laboratoria. Het is aanwezig wanneer je medicatie neemt, wanneer je gezuiverd water uit je kraan drinkt, wanneer je deze zin leest – en wanneer je hersens de woorden verwerken die je zojuist hebt gelezen.

Scheikundigen in het laboratorium weten precies met welke chemicaliën ze beginnen en kunnen precies achterhalen wat ze aan het einde hebben. Maar wat ze niet exact kunnen weten, is wat er tussendoor gebeurt. En juist hier ontstaan veel belangrijke vragen in de chemie. Hoe veranderden deze stoffen om te worden wat ze uiteindelijk vinden? En als er iets onverwachts gebeurt, welk deel van deze transformatie heeft dat veroorzaakt?

Om deze vragen te beantwoorden, kunnen we gebruik maken van computationele technieken die chemische reacties stap voor stap simuleren. Deze simulaties kunnen gedetailleerde antwoorden geven over hoe snel reacties verlopen, welke mogelijke uitkomsten er zijn en zelfs welke waarschijnlijk of onmogelijk zijn.

Hier gebruiken we dichtheidsfunctionaaltheorie (DFT), een zeer goed gevestigde computationele methode, om de eerdergenoemde vragen voor een aantal chemische reacties te beantwoorden. Deze reacties kunnen in twee categorieën worden ingedeeld. De eerste is organometaal katalyse, waarbij metaal bevattende stoffen chemische reacties versnellen die anders inefficiënt zouden zijn, of zelfs helemaal niet zouden plaatsvinden. De tweede categorie betreft supramoleculaire chemie, waarbij containervormige moleculen, zogenaamde *cavitands*, andere moleculen insluiten en leiden tot uniek gedrag dat niet in oplossing wordt waargenomen.

De berekeningen voor de organometalische reacties geven inzicht in hoe een reactie die door ijzer wordt gekatalyseerd verloopt, en beantwoorden de vraag waarom een reactie met goud tot een zeer specifiek product leidt. Diezelfde reactie met goud kan ook in een cavitand plaatsvinden, en wij laten zien hoe dat gebeurt. Tot slot onderzoeken we wat deze cavitanden nog meer kunnen doen – zoals het binden van moleculen die eigenlijk niet met een cavitand zouden moeten kunnen binden, en of ze een reactie kunnen katalyseren die normaal gesproken een enzym vereist.

List of Publications

The thesis is based on the following publications. They will be referred to in the text by their Roman numerals.

I. Mechanistic Studies on Iron-Catalyzed Dehydrogenation of Amines Involving Cyclopentadienone Iron Amine Complexes. Evidence for Stepwise Hydride and Proton Transfer

Srimanta Manna‡, Joannes Peters‡, Aitor Bermejo-Lopez, Fahmi Himo, Jan-E. Bäckvall.

ACS Catalysis, **2023**, *13*(13), 8477–8484.

‡ These authors contributed equally.

II. Computational Study of Gold-Catalyzed Cycloisomerization of Acetylenic Acids

Joannes Peters, Fahmi Himo.

Manuscript with supporting information.

III. Computational Studies of Alkyne-Acid Cycloisomerization in Gold-Functionalized Resorcinarene Cavitand

Joannes Peters, Fahmi Himo.

Chem. Eur. J., **2025**, e202404480.

IV. Recognition of hydrophilic molecules in deep cavitand hosts with water-mediated hydrogen bonds

Hua-Wei Guan, Yu-Jie Zhu, Joannes Peters, Oriana Brea, Fahmi Himo, Julius Rebek Jr., Yang Yu.

Chem. Commun., **2021**, *57*, 8147-8150.

V. On the Hydrolysis of Acetylcholine in a Resorcinarene-Based Cavitand

Joannes Peters, Oriana Brea, Fahmi Himo.

Manuscript with supporting information.

Author Contributions:

Paper I: Performed all calculations. Wrote the computational discussion section and computational supporting information.

Paper II: Performed all calculations. Wrote the manuscript and supporting information.

Paper III: Performed all calculations. Wrote the manuscript and supporting information.

Paper IV: Performed the conformational analysis on all guests except THF. Co-wrote the supporting information.

Paper V: Performed all mechanistic calculations, as well as conformer searching for all but one structure. Wrote the manuscript and supporting information.

Previous documents based on this work

This thesis is based on the author's halftime report titled "Modelling Reactions in Organometallic Catalysis and Resorcin[4]arene-based Cavitands", presented on May 8th, 2023 at the Department of Organic Chemistry, Stockholm University.

The introduction (**Chapter 1**) has received minor revisions.
The general theory chapter (**Chapter 2**) has received minor revisions.
Chapter 3 (**Paper I**) was included in the halftime report and has received minor revisions.
Paper II has been rewritten from the halftime report, and its summary (**Chapter 4**) was newly written.
Chapter 5 (**Paper III**) was not included in the halftime report, and as such has been written in its entirety for this thesis.
Chapter 6 (**Paper IV**) was included in the halftime report and has received minor revisions.
Paper V has been revised from the halftime report, and its summary (**Chapter 7**) was newly written for this thesis.

List of Acronyms and Abbreviations

atm	Atmosphere
B3LYP	Becke's 3-parameter exchange functional, Lee-Yang-Parr correlation functional
BJ	Becke-Johnson damping function
BO	Born-Oppenheimer
DFT	Density functional theory
DMBQ	2,6-dimethoxy-1,4-benzoquinone
DOF	Degree of freedom
FES	Free energy surface
GD3	Grimme's dispersion correction, 3rd generation
(m-)GGA	(meta-)Generalised gradient approximation
HF	Hartree-Fock
HK	Hohenberg-Kohn
KIE	Kinetic isotope effect
KS	Kohn-Sham
LDA	Local density approximation
LSDA	Local spin-density approximation
NCI	Non-covalent interaction
NMR	Nuclear magnetic resonance
QM	Quantum mechanic(al)
PMP	Para-methoxy phenyl
RDS	Rate-determining step
(q-)RRHO	(quasi-)Rigid rotor harmonic oscillator
SMD	Solvation model based on density
THF	Tetrahydrofuran
TM	Transition metal
TMANO	Trimethylamine N-oxide
TMA	Trimethylamine
TS	Transition state

Table of Contents

1. Introduction

It is hard to overestimate the importance and impact that chemistry has had on modern society, and the significance it will bear on the future. From advancement of modern medicine to developing novel industrial processes and synthesising advanced functional materials, chemistry has an undeniably large legacy that will only continue to grow. With the ever-increasing human population, the advent of mass consumerism and the impending threats of climate change, the problems that chemistry is expected to tackle have grown in size and diversified in nature.

Experimental chemistry has seen major improvements in methodology over the last century.[1,2] Nonetheless, there are still many challenging tasks. Chief among these include mechanistic studies of chemical reactions, the sequence of events during the transformation of reactants to products. Moreover, the isolation of high-energy intermediates continues to be a very challenging task and assigning plausible mechanisms remains subject to interpretation of circumstantial evidence to some extent.

In tandem with the modernising world, a new tool for chemical research has seen a relentless surge in popularity: computational chemistry. Accompanied by ever-faster hardware and increasingly efficient methods and algorithms, computational chemistry has evolved into a complementary and highly practical method of pursuing chemical research. [3,4] In particular, Density Functional Theory (DFT) has grown to the forefront of quantum chemical methodology for modelling small or medium sized chemical systems owing to its good accuracy/cost balance.[5] With DFT one can make both qualitatively and quantitatively meaningful assessments of a large variety of chemical systems and reactions.

In this thesis, DFT calculations are employed to study a number of reactions. These can be distinguished into two categories: homogeneous organometallic catalysis and supramolecular chemistry. Of the five cases presented here, two are mechanistic studies of metal-catalysed reactions, and three are investigations into the binding and reactivity of host-guest systems.

1.1. Homogeneous Catalysis

Catalysts are chemical substances that enhance a reaction rate without being consumed themselves. Although the catalyst can participate in the reaction itself, it is always regenerated at the end of the reaction. There are three main types of catalysts, namely homogeneous catalysts, heterogeneous catalysts and biocatalysts. The focus of the relevant chapters in this thesis is on the first. Homogeneous catalysis involves reactions where all the components are in the same phase, usually the solvated state. The importance of homogeneous catalysis in modern society is very well established and will only continue to grow with the challenges imposed on the modern world.[6–9] Computational chemistry too, has a great role to play in solving these challenges.[10,11] The calculations of free energy profiles for catalytic cycles give insights into intricate details of the reaction mechanism, as well as giving complementary insights into experimental observations. We demonstrate such synergy in **Chapter 3** where we use DFT to investigate the reaction mechanism of the dehydrogenation of amine substrates using a cyclopentadienone iron carbonyl catalyst. The calculations give additional insights into experimental observations made for the reaction mechanism.

Quantum chemical calculations are also capable of unravelling reaction mechanisms by themselves. An example is given in **Chapter 4**, where DFT was used to elucidate the mechanism of cycloisomerisation of γ-alkyne acids using a gold catalyst. In this case, the calculations not only determine the reaction mechanism, but also the origins of the regio- and stereoselectivity observed experimentally.

1.2. Host-guest chemistry

Host-guest chemistry is the study of chemical systems where molecules are held together through non-covalent bonds. Examples of these bonding types include hydrogen bonds, van der Waals forces and ionic bonds. In these systems, a large molecule (the host) can form a complex with one or several smaller molecules inside of it (guests). Within the host lies a confined environment with limited volume where guests are shielded from solvent.[12,13] These environments have been shown to enable a range of behaviours deviating from the same systems in solution, such as inverted selectivity, reaction rate acceleration and even catalysis.[14,15]

Of particular interest for the present work is a class of hosts known as cavitands, specifically those based on resorcin[4]arene. These container-shaped molecules have a cavity capable of binding guests of complementary sizes, much like enzymes having affinity for molecules of particular sizes. Cavitands have also been functionalised with transition metals to combine the homogeneous organometallic chemistry outlined above with the confinement effects of the cavitand.[16] One such example is studied in **Chapter 5**, where a gold-functionalised cavitand was used for the cycloisomerisation reaction described in **Chapter 4**. The calculations examine different size-reactivity patterns from different substrates, as well as the influence the cavitand's structure has on the binding and reactivity of the reaction.

Developments in synthetic methods have enabled the construction of water-soluble cavitands, which have very interesting binding properties.[17–19] A study of such binding properties for a resorcin[4]arene cavitand is described in **Chapter 6**, where the most favourable binding modes of a number of hydrophilic guests in a hydrophobic cavitand were investigated.

Although binding studies have a very long history of investigation, significantly less is known about the reactivity alterations that cavitands can provide. **Chapter 7** describes the hydrolysis of acetylcholine in aqueous solution and in a water-soluble cavitand. The calculations aim to discern whether the cavitand can possibly catalyse the hydrolysis reaction.

1.3. Aims

The thesis aims to advance mechanistic understanding of various reactions in both organometallic catalysis and supramolecular host-guest chemistry through DFT calculations. These calculations contribute in three possible ways: i) by evaluating the feasibility of previously proposed mechanisms, like in the case of the cycloisomerisation of acetylenic acids to lactones, both in solution (**Chapter 4**) and in a supramolecular cavitand (**Chapter 5**); ii) in collaboration with experimentalists to add further insight, such as combining calculations with kinetic isotope effect (KIE) experiments (**Chapter 3**) or nuclear magnetic resonance (NMR) experiments (**Chapter 6**); and iii) as a tool to predict mechanisms ahead of experiments, as for example the hydrolysis of acetylcholine in a resorcinarene-based cavitand (**Chapter 7**), and thereby suggesting new experimental avenues.

2. General Theory

Computational mechanistic studies rely on the free energy of a molecular system as the main source of information for a given system. The free energy can provide insight into the thermodynamical aspects of chemical reactions as well as their kinetic aspects. There are many methods that can calculate the energy of chemical systems, depending on the accuracy required and the complexity of the model, among other reasons. These methods range from classical molecular mechanics to semi-empirical methods to full quantum mechanical (QM) methods. The method of choice for all papers presented in this thesis is DFT. In this chapter, a brief description will be given on how DFT can be used to calculate the energy, as well as the corrections to the resulting energy needed to obtain more accurate results. Finally, this chapter will elaborate on how the energy of a molecular system can be related to observable properties such as kinetics and selectivity.

2.1. Density Functional Theory

In DFT, the electron density of the molecule serves as the fundamental variable. The electron density of a system is defined as follows:

$$\rho(r) = N \int \dots \int |\Psi(r_1, r_2 \dots r_N)|^2 \, dsdr_2 \dots dr_N \qquad (1)$$

Where N is the number of electrons, r represents the coordinates of each electron, and s is the spin variable. The resulting density has a number of interesting properties, such as the formation of cusps at the nuclei, forming a nuclear constellation.[20]

The theoretical foundations of DFT are the Hohenberg-Kohn (HK) theorems.[21] The first HK theorem states that the electron density determines a unique external potential through which the electrons move and, by consequence, the wavefunction and ground state properties. The second HK theorem states that DFT follows the variational principle similarly to how it is

applied to other QM methods. This means that the energy obtained from a guess density is an upper limit to the true ground state energy.

The energy of a molecular system is defined by the following expression:

$$E[\rho(r)] = T[\rho(r)] + V_{Ne}[\rho(r)] + V_{ee}[\rho(r)] + V_{NN}(R_{ij}) \quad (2)$$

Where $T[\rho(r)]$ is the kinetic energy of a system of interacting electrons, $V_{Ne}[\rho(r)]$ is the attractive potential between the nuclei and electrons, $V_{ee}[\rho(r)]$ is the electron-electron repulsion potential, and $V_{NN}(R_{ij})$ is the repulsive potential between the nuclei. Within the Born-Oppenheimer (BO) approximation, the nuclear and electronic wavefunctions are separated from each other due to the large differences in velocities between the nuclei and electrons. Since $V_{NN}(R_{ij})$ is only dependent on nuclear positions, it will be a constant for a fixed nuclear geometry.

The main issue with early attempts at developing DFT stemmed from the inaccuracy associated with computing the interaction of the electrons. Kohn and Sham would address this issue through the development of the Kohn-Sham (KS) formalism.[22] Here, the electron-electron repulsion $V_{ee}[\rho(r)]$ is split into two components: the classical Coulombic repulsion, $J[\rho(r)]$, and all nonclassical energy contributions. Furthermore, they redefined the kinetic energy of a system of interacting particles as the kinetic energy of a system of noninteracting particles and an additional term. These changes to *(2)* lead to the revised expression:

$$E_{el}[\rho(r)] = T_{ni}[\rho(r)] + V_{Ne}[\rho(r)] + J[\rho(r)] + E_{xc}[\rho(r)] \quad (3)$$

with

$$E_{xc}[\rho(r)] = (T[\rho(r)] - T_{ni}[\rho(r)]) + (V_{ee}[\rho(r)] - J[\rho(r)]) \quad (4)$$

Where $T_{ni}[\rho(r)]$ describes the kinetic energy of a system of noninteracting electrons and $E_{xc}[\rho(r)]$ is the exchange-correlation potential. The exchange-correlation potential contains all nonclassical terms for the kinetic energy of the system as well as part of the electron-electron repulsion. The advantage of this approach is that all but the exchange-correlation term can be computed exactly. Unfortunately, no exact expression exists for the exchange-correlation energy. As such, one needs to approximate the energy using an exchange-correlation functional.

Functionals for DFT can generally be divided into three categories: the Local Density Approximation (LDA), Generalised Gradient Approximation (GGA) functionals, and meta-Generalised Gradient Approximation (m-GGA) functionals. In addition, GGA and m-GGA functionals can be subclassed as either 'pure' or 'hybrid'. Hybrid functionals parametrise the exchange energy by incorporating a fraction of exchange energy from Hartree-Fock (HF), whereas pure functionals do not. All publications in this thesis employ a very popular hybrid GGA functional named B3LYP. This functional has three sources for its exchange energy expression, namely the Local Spin Density Approximation (LSDA), exact HF exchange energy, and an exchange term developed by Becke.[23] The correlation functional on the other hand comes from two sources. One is correlation energy derived from the LSDA and the other one is from a term developed by Lee, Yang and Parr.[24] These combined give rise to the full expression of the B3LYP functional:

$$E_{xc}^{B3LYP}[\rho(r)] = (1-a)E_x^{LSDA} + aE_x^{HF} + bE_x^B + (1-c)E_c^{LSDA} + cE_c^{LYP} \qquad (5)$$

The parameters a, b and c weigh the contributions of the aforementioned exchange and correlation energy sources. The values of these parameters are $a = 0.20$, $b = 0.72$, and $c = 0.81$, which were originally obtained through fitting to experimental data for atomisation and ionisation energies, among other properties.

The capabilities of B3LYP have been well-tested throughout the last three decades. Its use as a generally applicable functional with a good cost/accuracy ratio has secured its immense popularity, and it continues to be one of the most used functionals.

2.2. Dispersion energy corrections

No method is perfect, and B3LYP is no exception. One limitation is the treatment of non-uniform medium-range interactions stemming from London dispersion forces. These weak but significant forces arise from fluctuations in electron density and electron correlation. Although individually small, these inaccuracies accumulate significantly in large systems, impacting both geometries and energies.[25] To address this issue, Grimme introduced a dispersion correction term,[26] which accounts for the medium-range dispersion forces through the following general equation:

$$E_{disp}^{D} = -\frac{1}{2}\sum_{A\neq B}\sum_{n=6,8,\ldots} s_n \frac{C_n^{AB}}{r_{AB}^n} f_{damp}(r_{AB}) \quad (6)$$

Where A and B represent different atoms, s_n are scaling factors that depend on the choice of functional, C_n^{AB} are the dispersion coefficients for all atom pairs in the system, and r_{AB} are the internuclear distances. Although in theory the correction could be applied for any number of terms, Grimme's third-generation dispersion (D3) correction, the method used in this thesis, only includes *n=6* and *n=8*. $f_{damp}(r_{AB})$ is the damping function used in order to counteract the singularities occurring at $r_{AB} = 0$. The Becke-Johnson (BJ) damping function is used in all works presented here.[27] Combining the BJ damping function with the D3 term leads to the following expression for the dispersion energy:

$$E_{disp}^{D3(BJ)} = -\frac{1}{2}\sum_{A\neq B} s_6 \frac{C_6^{AB}}{r_{AB}^6 + [f_{damp}(r_{AB}^0)]^6} + s_8 \frac{C_8^{AB}}{r_{AB}^8 + [f_{damp}(r_{AB}^0)]^8} \quad (7)$$

With

$$f_{damp}(r_{AB}^0) = a_1 r_{AB}^0 + a_2 \quad (8)$$

and

$$r_{AB}^0 = \sqrt{\frac{C_8^{AB}}{C_6^{AB}}} \quad (9)$$

Where a_1 and a_2 are two additional free fit parameters introduced to fine-tune the damping of the functional.

2.3. Free energy corrections

Although the electronic energy described above constitutes a major portion of a system's internal energy, additional corrections are required to obtain an accurate energy. The following section outlines how the Gaussian software computes the Gibbs free energy. [28]

The Gibbs free energy is defined as follows:

$$G = H - TS \quad (10)$$

Where G is the total Gibbs free energy, H is the enthalpy, T is the temperature and S is the entropy of the system. In Gaussian, the correction to enthalpy is defined as follows:

$$H_{corr} = E_{tot} + k_b T \tag{11}$$

Where E_{tot} is the total electronic energy, a summation of the electronic energy, the zero-point energy, and thermal energy contributions from the translational, vibrational, and rotational motions. k_b is the Boltzmann constant.

The entropy of the system is dependent on the number of accessible states. A molecule with N atoms has $3N$ degrees of freedom (DOF). Of these, three constitute the translational DOFs. For nonlinear molecules, another three account for the rotational DOFs. The remainder are the vibrational DOFs, of which there are *3N-6* in a nonlinear molecule. The thermal corrections for each DOF that contribute to the free energy are calculated using an equation for each component. The vibrational contributions are determined within the Rigid-Rotor Harmonic Oscillator approximation (RRHO), which assumes that the vibrational and rotational energies are decoupled from one another—i.e., a molecule's rotations do not influence its vibrations and vice versa.

Although the RRHO approximation is a generally good one, it introduces an error in the treatment of low-frequency vibrational modes. Using this approximation, the vibrational entropy is calculated by the following equation:

$$S_{vib} = R\sum_{i=1}^{3N-6(7)}\left[\frac{h\omega_i}{k_bT\left(e^{\frac{h\omega_i}{k_bT}}-1\right)} - ln\left(1-e^{-\frac{h\omega_i}{k_bT}}\right)\right] \tag{12}$$

Where R is the ideal gas constant, ω_i is the vibrational frequency and h is Planck's constant.[29] An inaccuracy associated with the equation above stems from the first term in the brackets, which contains the frequency in the denominator. This creates an asymptote towards infinity as $\omega_i \to 0$, leading to erroneously large contributions to the entropy from *soft* vibrational modes.

To account for this inaccuracy, most research projects presented here use the quasi-Rigid-Rotor Harmonic Oscillator (q-RRHO) approximation instead.[30] In this approximation, a cut-off value is introduced, below which any vibrations will be treated as rotations instead. The value of the cut-off is 100 cm^{-1} in all works here.

Incidentally, the calculation of the vibrations allows us to verify whether a calculated geometry is a minimum (no imaginary frequencies) or a first-order transition state (one imaginary frequency).

2.4. Solvation models

All the reactions discussed in this thesis are performed in solution, and thus the treatment of their solvents requires consideration. The interaction between the solute and the solvent highly depends on the nature of the solvent itself. Nonpolar solvents, such as chloroform and toluene, interact with the solute through dispersion interactions. Highly polar solvents on the other hand, such as acetonitrile, THF or water, can interact with the solute through stronger dipole interactions. Acetonitrile and THF are known to be able to coordinate to free coordination sites in transition metal (TM) complexes, for example. Water is a particularly complicated solvent to model owing to its ability to form complex hydrogen-bonding networks. Lastly, in reactions such as hydrolysis, the solvent directly participates in the reaction as a reagent (see, for example, **Paper V**).

Since the *explicit* modelling of even a few solvent molecules can quickly become an overly complex task, it is instead more practical to use a simpler approximation in which the solvent is treated as a homogeneous polarisable continuum. In these methods, the solute is placed in an electrostatic cavity, whilst the solvent is represented as a dielectric medium.[29] The charges of the solute are allowed to interact with this dielectric medium, recursively polarising each other until convergence is achieved. Models that solely employ a continuum model are named *implicit* models, and they are sufficiently accurate for describing systems where the solvent only interacts with the solute weakly.

In the event that implicit modelling is insufficient, such as when strong solute-solvent interactions are present or where the solvent is a reactant, we can choose a middle way between an implicit and explicit model, where a small number of solvent molecules are modelled explicitly and the rest is approximated by a continuum. This style of model is called a *mixed* model.

2.5. *Energy surfaces and transition state theory*

A chemical reaction can be visualised as the geometric rearrangement of reagents into products, during which the energy of the reaction components changes. Due to the large number of coordinates changing during a typical chemical reaction, and the high number of dimensions associated with it, it is conventional to condense all dimensions into a single, one-dimensional graph. This graph, known as a Free Energy Surface (FES), displays a system's free energy as a function of a sequence of events, i.e., the process of converting reactants to products, with intermediate steps in between.

A deviation from an equilibrium geometry increases the energy of a molecule until a local maximum is reached, after which the energy will descend as the reaction reaches the product state. The structure associated with the local maximum in is named a transition state (TS), and it represents the minimal amount of energy required to overcome the barrier leading to the product. As such, it is also the limiting factor in a chemical reaction's rate. A typical reaction mechanism for a chemical reaction usually contains multiple steps and, by consequence, multiple transition states. The rate constant of an individual step, k, is calculated through the Eyring-Polanyi equation *(13)*:

$$k = \frac{\kappa k_b T}{h} e^{-\frac{\Delta G^{\ddagger}}{RT}} \qquad (13)$$

Where $\Delta G^{\ddagger}$ is the free energy of the transition state, R is the ideal gas constant, and κ is the transmission coefficient, which will always assume a value of 1 in this thesis. Each individual step in a reaction has its own rate, as does the reverse reaction from product back to reactant.

When a chemical reaction has consecutive multiple steps, the overall rate is determined by the energy of the highest-energy transition state relative to the energy of the lowest-energy minimum preceding it. The step with this transition state is called the *rate-determining step* (RDS). It is important to note that the individual rate constant of a step does not determine whether it is rate-determining.

2.7. Computational details

All calculations were performed using the dispersion-corrected B3LYP-D3(BJ)[23,24,26,27] functional (see **Chapters 2.1 & 2.2**) as implemented in the Gaussian16 software package, revision C.01.[31] The geometries were optimized using the 6-31G(d,p) basis set for all atoms, except for any transition metal atoms, for which the LANL2DZ (iron, **Paper I**) or the SDD basis set (gold, **Papers II&III**, and silver, **Paper III**) were used. The resulting electronic energies were further refined by single-point calculations on the optimized structures using the larger 6-311+G(2d,2p) basis set for all atoms except transition metal atoms, for which their original basis sets were maintained. Frequency calculations were carried out at the same level of theory as the optimizations to verify the nature of the obtained stationary points. Gibbs free energy corrections were evaluated using either the quasi-rigid rotor harmonic oscillator (q-RRHO) approximation with a cut-off value of 100 cm^{-1} at a temperature of 298 K (**Papers II-V**), or the RRHO approximation as implemented in Gaussian16 at a temperature of 353 K (**Paper I**).[30] Solvation corrections were carried out using the SMD implicit solvation method,[32] either as single-point energy calculations (**Papers II-V**) or by optimizing in solution (**Paper I**). Standard state corrections were added to account for the change of a 1 atm gas to a 1 M solution state. Hence, a correction term of -RT ln (1/24.5) = +1.9 kcal/mol was added to the energies of all species except for the solvents acetonitrile (**Paper II**) and chloroform (**Paper III**), for which corrections of -RT ln (1/(24.5x19.1)) = +3.6 kcal/mol and
-RT ln (1/(24.5x12.5)) = +3.4 kcal/mol were added, respectively.

For **Paper IV**, non-covalent interaction (NCI) analysis was carried out for the identification and classification of non-covalent interactions between the cavitand host and the guests, as well as for bridging water molecules. The calculations were carried out with NCIPlot 4.0.1, [33] using the promolecular approximation, and cutoff values of 0.5 au for density and 1.0 au for reduced density gradient.

3. Iron-Catalysed Dehydrogenation of Amines (**Paper I**).

3.1. Introduction

Dehydrogenation and hydrogenation are important classes of reactions in organic synthesis due to their high functional group tolerance and, depending on the catalyst used, low cost.[34–37] Traditionally, (de)hydrogenation catalysts are made of expensive noble metals such as iridium or palladium, prompting interest in the search for cheaper, more abundant alternatives.

One such alternative is (cyclopentadienone)iron carbonyl catalysts. These were first synthesised by Repper and Vette in 1953,[38] and other analogous complexes including Knölker catalysts[39] and complexes developed by Funk[40] were synthesised later. The use of these complexes as catalysts for (de)hydrogenation reactions is well known ever since Casey and Guan reported the use of Knölker-type catalysts for the hydrogenation of ketones.[41]

One other reaction of interest is the dehydrogenation of amines to imines using iron catalysts, reported by Casey and Guan.[42] Despite having an extensive history of investigation,[43] some details of the reaction mechanism remain unclear. In particular, there is conflicting literature precedent over whether the dehydrogenation of amines (as well as its reverse process) occurs in a stepwise or concerted fashion. On the one hand, von der Höh and Berkessel found that the hydrogenation of imines proceeds through a stepwise mechanism consisting of a fast proton transfer followed by a rate-limiting hydride transfer. [44] Renaud, Poater and co-workers on the other hand have published a series of articles describing the hydrogenation reaction with a concerted mechanism.[45–48] Benaglia and co-workers found that the reaction proceeds through a concerted but asynchronous mechanism.[49] Lastly, Hopmann found a concerted mechanism for the hydrogenation of cyclic imines.[50]

In order to discern whether the dehydrogenation reaction occurs in a concerted or stepwise fashion, a combined experimental and computational mechanistic study of the dehydrogenation of amines using (cyclopentadienone)iron carbonyl catalysts was carried out. A short summary of the experimental results will be given here before the main focus will be laid on the computational results.

3.2. Results and discussion

3.2.1. Experimental results

There are two important experimental results that merit discussion prior to the computational section. The first is the isolation of air-stable iron-amine intermediate complexes. The second is a series of inter- and intramolecular KIE experiments.

The (cyclopentadienone)iron tricarbonyl complex **I** is activated through oxidative elimination of a carbonyl ligand using trimethylamine N-oxide (TMANO). The resulting 16-electron complexes **II** can subsequently coordinate an amine before the dehydrogenation takes place (Scheme 3.1). The isolation of the resulting iron-amine complexes is difficult, as these complexes usually decompose in air. After several attempts with multiple amines, iron-amine complex **III** was isolated and characterised by ^{1}H and ^{13}C NMR analysis, as well as X-ray crystallography (Figure 3.1).

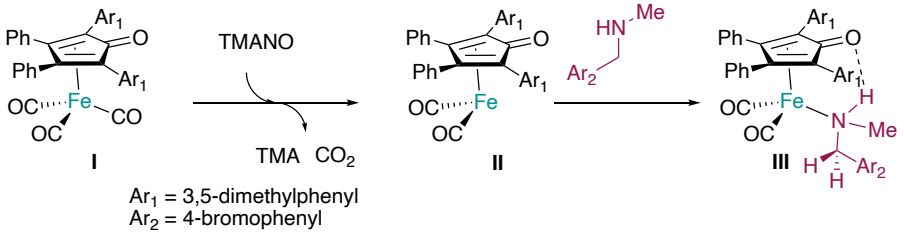

Scheme 3.1. *Activation of **I** by TMANO, and the subsequent coordination of an amine to form **III**.*

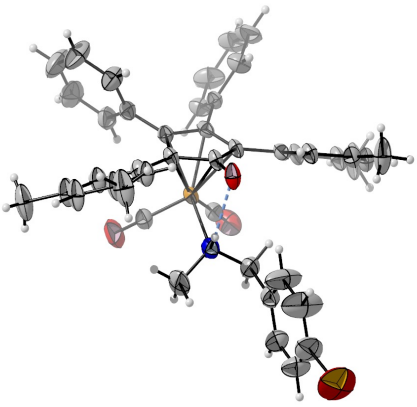

III

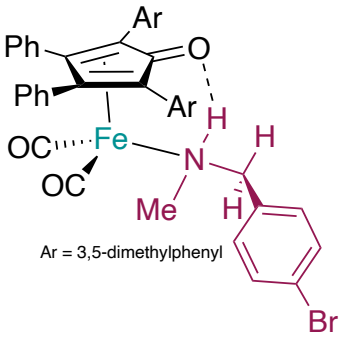

III

Figure 3.1. *Structures obtained of iron-amine complex* ***III*** *with X-ray crystallography.*

More importantly, however, KIE experiments give strong evidence for a stepwise mechanism with the loss of the β-hydride as the RDS (Scheme 3.2). (Deuterated) amines **1A-D** were prepared for a series of intermolecular KIE experiments. The combined reaction of **I** with **1A** and the N- and C-deuterated amine **1B** gave a KIE of 3.77 ± 0.15. Interestingly, the value obtained is almost identical to the KIE of the comparison between the rate of **1A** and **1C** with **I** (3.72 ± 0.13). These combined results indicate that the influence of the amine proton on the resulting rate is negligible compared to the influence of the β-hydride atom. The comparison of the reaction rates between the non-deuterated amine **1** and the N-deuterated amine **1D** in separate experiments gave a KIE of 1.22 ± 0.14, indicating a very small effect of the N-H cleavage in comparison to the C-H cleavage.

A final important result is an intramolecular KIE experiment between **1A** and the amine with only one deuterated β-hydride atom (**1E**). The product distribution from reacting **I** with **1A** and **1E** in the same experiment gave a KIE of 2.44 ± 0.14. The obtained value is attributed to a secondary KIE, and the fact that it is smaller than the observed KIE for C-H cleavage of **1C** leads to the conclusion that the formation of the iron-amine complex prior to the dehydrogenation step is not the RDS.

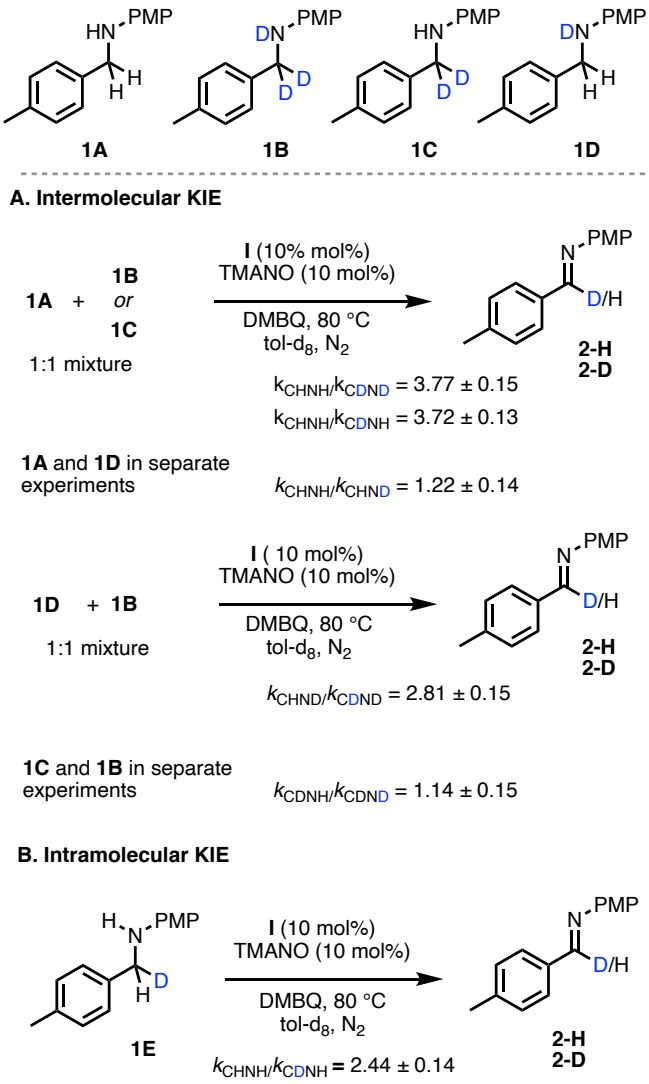

Scheme 3.2. *Kinetic isotope effect studies.*

The KIE experiments and the isolation of **III** provide the following insights:

- The reaction between an amine and activated, 16-electron complexes such as **II** yields iron-amine complexes prior to the dehydrogenation reaction.
- The cleavage of the C-H bond and N-H bond occurs in a stepwise fashion.
- The hydride transfer is involved in the RDS.

- The proton transfer is very fast compared to the hydride transfer, regardless of the sequence of the steps. Moreover, the N-H cleavage does not occur during the RDS.
- The formation of the iron-amine complex prior to dehydrogenation is not the RDS.

3.2.2. Computational results

DFT calculations were employed in to order to elucidate the reaction mechanism. The reaction between amine **1A** and Funk-type catalyst **I** was studied as a representative example The calculations begin from the activated catalyst **II**, and the obtained mechanism and free energy profile are shown in Scheme 3.3 and Figure 3.2, respectively.

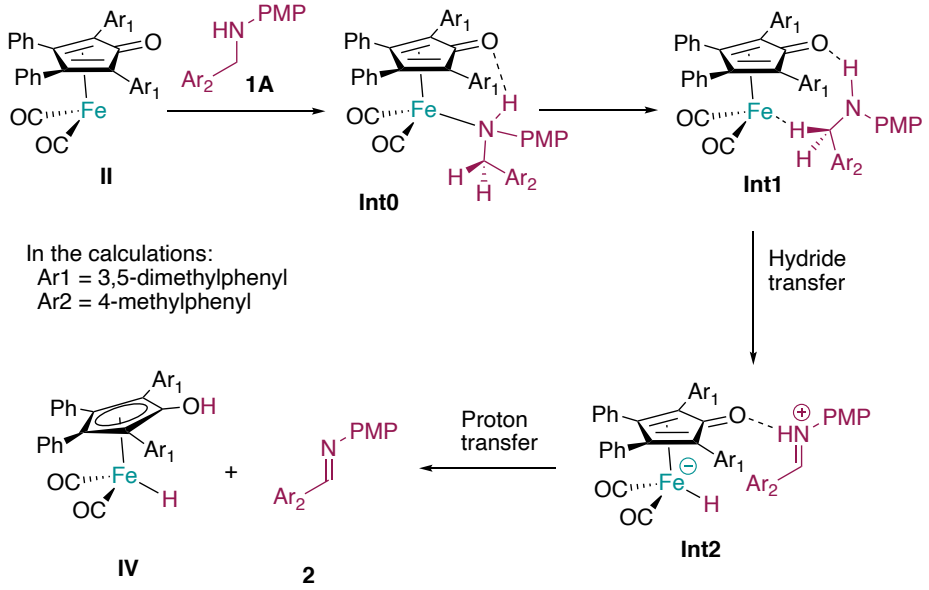

Scheme 3.3. *Mechanism obtained from DFT calculations.*

The mechanism is initiated by the complexation of **1A** and **II** to form the iron-amine adduct **Int0**. The calculations show that amine **1A** binds by as much as 22.1 kcal/mol, and that it is the resting state for the catalyst. Such iron-amine complexes have been calculated before,[48,50] and analogous species with iron-oxygen bonds have an even larger precedent in literature.[51–56] Moreover, the calculated geometry of **Int0** is in excellent agreement with the X-ray crystal structures of the isolated iron-amine complex **III** (Figure 3.1). Complex **Int0** undergoes a

coordination change to bind to catalyst **II** with the hydride atom rather than the nitrogen atom. Such a change in coordination was calculated to yield complex **Int1** at an energetic cost of +27.1 kcal/mol. Similar complexes have also been reported previously by other groups.[45–48,50–57]

From **Int1**, the C-H bond is cleaved to give an iminium-metal hydride ion pair **Int2**. This is the rate-determining step of the reaction and has a barrier of 30.0 kcal/mol. This barrier height is in line with the experimental conditions (24hr reaction at 80°C). The iminium-metal hydride ion pair **Int2** was located 6.4 kcal/mol downhill from **TS1** i.e., +23.6 kcal/mol relative to **Int0**. Calculations of such an ion pair complex were previously reported by von der Höh and Berkessel.[44]

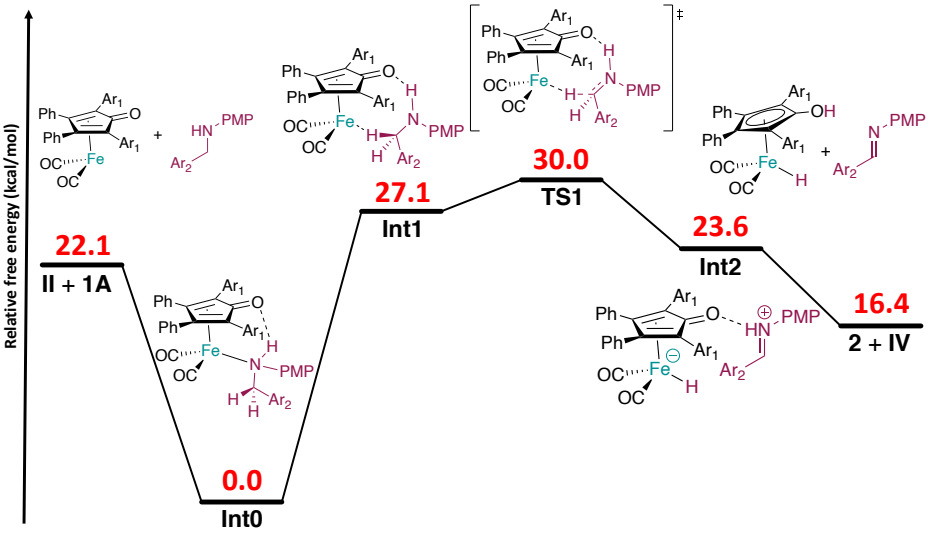

Figure 3.2. *Calculated free energy profile.*

Finally, a proton transfer from the iminium to the cyclopentadienone ligand occurs, resulting in the formation of the iminium product **2** and complex **IV**. Upon optimising the transition state for this step (**TS2**), the barrier was calculated to be 0.1 kcal/mol lower than the preceding ion pair. Refinement of the electronic energy changed increased the barrier to +0.1 kcal/mol, and the addition of corrections to free energy lowered energy down to -4.1 kcal/mol relative to **Int2**. The negative barrier is of course an error in the calculations, but it does demonstrate that the proton transfer is a much faster step than the hydride transfer.

The ion pair **Int2** is consistent with Berkessel's calculations[44] on the hydrogenation of imines with Knölker-type catalysts (i.e., the reverse reaction), and the higher barrier of the

hydride transfer compared to the proton transfer is in line with the observed KIE. It is very important to note that **Int2** could only be calculated when optimised using the SMD implicit solvation model. Attempts to optimise the ion pair complex in the gas phase resulted in a concerted mechanism where the proton transfer and the hydride transfer occurs in a single step.

Given the very low barrier associated with the proton transfer step, it cannot be ruled out that the stepwise mechanism obtained here is the result of the specific choice of substrate and catalyst. A different choice of amine substrate or catalyst ligands might result in a concerted mechanism.

3.3. Conclusions

The mechanism of amine dehydrogenation using (cyclopentadienone)iron carbonyl catalysts was investigated through both experimental and computational means. An iron-amine adduct was isolated and characterised by NMR and X-ray crystallography. KIE experiments suggest a stepwise mechanism with a rate-limiting hydride transfer step and a fast proton step. DFT calculations corroborate this picture, demonstrating a hydride transfer leading to an iminium-metal hydride ion pair complex. From there a proton transfer occurs to yield the final products.

4. Gold-Catalysed Cycloisomerisation of Acetylenic Acids in Solution (**Paper II**).

4.1. Introduction

The use of gold in homogeneous catalysis has experienced a massive increase over the last few decades.[58–63] In particular, gold has proven to be an excellent means to activate alkyne triple bonds owing to the high π-acidity of gold.[64–67] Among the many possible functionalisations of alkynes, the cycloisomerisation of acetylenic acid to enol-lactones stands out as a reaction of great interest.[68,69] These compounds, especially sesquiterpene lactones, have various uses in the medicinal field,[70–72] as well as applications in polymer chemistry.[73] The lactone motif is also very prominent in chemical signalling between organisms.[74]

One interesting method for performing this cycloisomerisation reaction was reported by Pale and co-workers, where the use of gold(I) chloride **3** and potassium carbonate **4** in catalytic amounts allowed for the cycloisomerisation of a wide range of substrates at room-temperature (Scheme 4.1).[75] This reaction showed both high regioselectivity towards γ-lactone products, and upon substituting the alkyne with various groups, a near-universal stereoselectivity towards (*Z*)-*exo*-alkylidene γ-lactones was observed. The only exception to this selectivity trend observed was the case of the *n*-butyl substituted **5d**, for which a 1:1 *E*/*Z* mixture of γ-lactones was obtained.

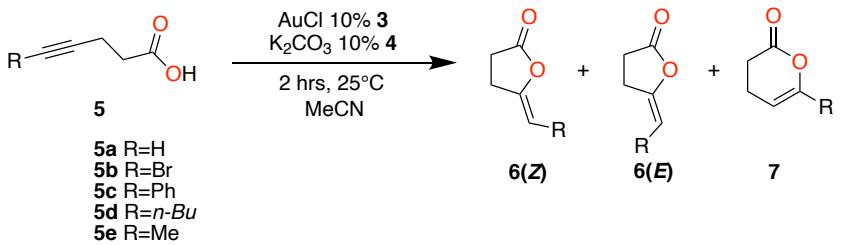

5

5a R=H
5b R=Br
5c R=Ph
5d R=*n-Bu*
5e R=Me

6(*Z*) **6(*E*)** **7**

Scheme 4.1. *Cycloisomerisation of acetylenic acids to their products considered here.*

Despite the many attractive qualities of the above cycloisomerisation method and its many subsequent applications, the reaction mechanism has not been investigated to this day. In fact, mechanistic studies on the gold-catalysed cycloisomerisation of acetylenic acids are sparse in the literature,[76–78] in spite of the evident need for mechanistic information to fully exploit the reaction's capabilities.

Here, DFT calculations were employed to investigate the cycloisomerisation of acetylenic acids to enol-lactones as carried out experimentally by Pale and co-workers.[75] The resulting mechanism is used to discern the origins of both the regio- and stereoselectivity of the reaction.

4.2. Results and discussion

Pale and co-workers have previously proposed a mechanism [75] for the reaction (Scheme 4.2.) where initially, the acetylenic acid substrate is deprotonated by catalytic amounts of **4** to yield a carboxylate substrate and $KHCO_3$. Moreover, the active catalyst for the reaction is Au^+—i.e., the chloride was dissociated from **3**. The resulting carboxylate coordinates to the gold ion before cyclisation takes place. This can occur through either a 5-*exo*-dig or a 6-*endo*-dig pathway. Additionally, the 5-*exo*-dig cyclisation can occur through either a *syn*- or *anti*-periplanar addition to the alkyne which, in the case of internal alkynes, leads to (*E*)- and (*Z*)-stereoisomers, respectively (Figure 4.1). The cyclisation leads to a gold alkylidene lactone intermediate, which subsequently undergoes protodeauration. For this step to take place, a new substrate molecule acts as a proton source, which forms both the product as well as a new carboxylate molecule for the next cycle.

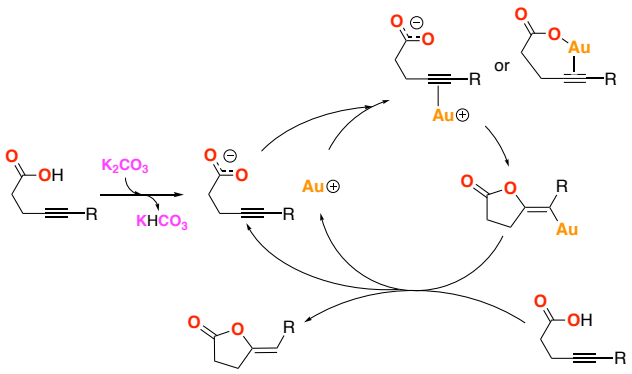

Scheme 4.2. *Previously proposed reaction mechanism cycle for gold-catalyzed cycloisomerization of acetylenic acids. [75]*

The mechanism originally proposed by Pale and co-workers was calculated with some modifications (Scheme 4.3) to reflect some reasonable constraints in the computational setting. In particular, since carboxylic acids can form dimers through complementary hydrogen bonds, and carboxylate anions can engage in proton sharing with an acid molecule, they were modelled accordingly as dimers and acid-carboxylate complexes, respectively. In addition, care was taken not to leave vacant coordination sites on the gold ion, either by explicitly modelling solvent molecules as ligands, or by coordinating the alkyne or carboxylate group from an acid or carboxylate group, respectively. Lastly, the energies of the initial deprotonation of **5a** and the dissociation of chloride from **3** were not considered explicitly in the calculations.

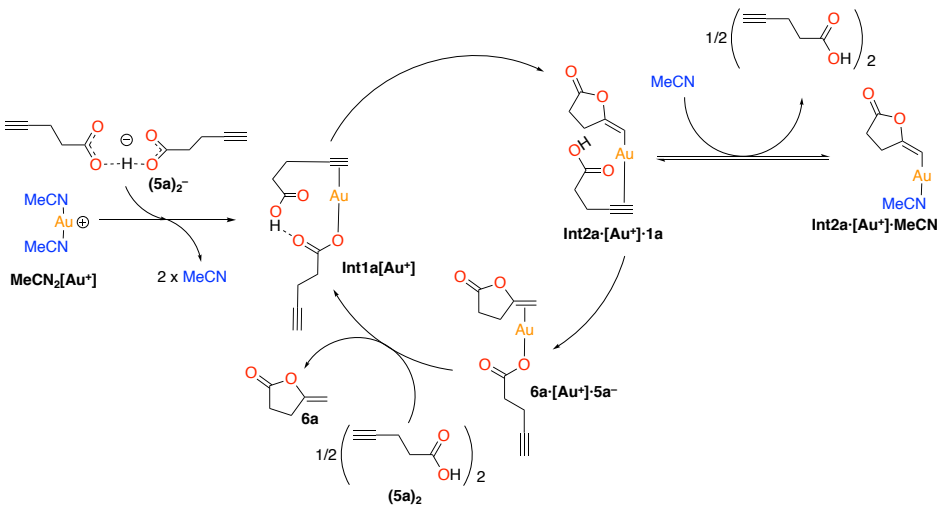

Scheme 4.3. *Modified catalytic cycle for the cycloisomerization of* ***5a*** *acid by* Au^{+}.

The free energy profile for the cycloisomerisation of **5a** by Au^{+} is shown in Figure 4.1. It was found that the lowest-energy pathway is associated with the 5-*syn*-*exo*-dig cyclisation. This preference is attributed to the fact that during cyclisation, a simultaneous proton transfer occurs from the acetylenic acid to the carboxylate ligand. The 5-*syn*-addition is well oriented for this TS, whereas the 5-*anti*-*exo*-dig and the 6-*endo*-dig TSs are very strained, which raises their respective barriers. The cyclisation step was found to be selectivity-determining as it was calculated to be an irreversible step at which all three pathways diverge. The subsequent protodeauration step was calculated to be rate-determining for the cycloisomerisation reaction.

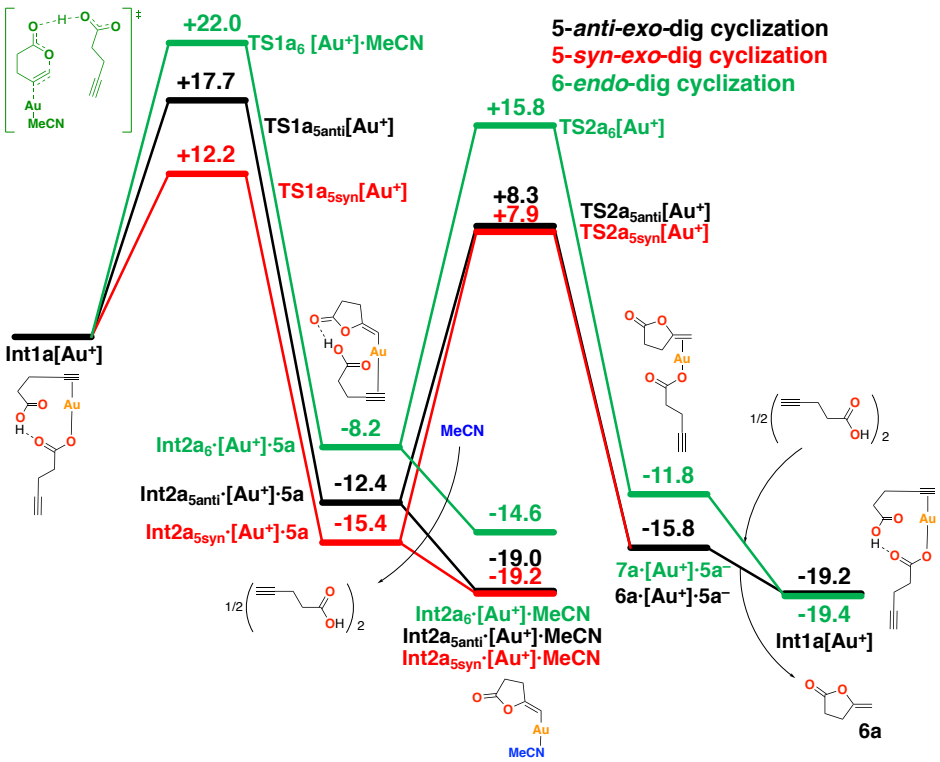

Figure 4.1. *Calculated free energy profile for the cycloisomerization of 5**a** by Au⁺. Energies are in kcal/mol.*

Although the mechanism reproduces the reactivity of the reaction reasonably well, it does not predict the correct selectivity. This is because experimentally, upon substituting pent-4-ynoic acid to obtain the bromide-substituted **5b** and the phenyl-substituted **5c**, the cycloisomerisation resulted in the exclusive formation of their (*Z*)-*exo*-alkylidene γ-lactone products **6b(*Z*)** and **6c(*Z*)** (Scheme 4.1).[75] The formation of such products proceeds through a 5-*anti*-*exo*-dig cyclisation. However, in the case of both **5b** and **5c**, the calculations showed that the 5-*syn*-*exo*-dig is still the lowest in energy (Table 4.1), which leads to the corresponding (*E*)-stereoisomer not observed experimentally.

Table 4.1. *Relative energies (in kcal/mol) of 5-exo-dig cyclisation TSs of* ***5b*** *and* ***5c*** *by* Au^+.

Substrate	$TS1_{5syn}[Au^+]$	$TS1_{5anti}[Au^+]$
5b	0.0	+5.3
5c	0.0	+2.2

A second analogous mechanism was calculated, where AuCl was the active catalyst, i.e., the chloride was not dissociated. The resulting catalytic cycle and free energy profile associated therewith are given in Scheme 4.4 and Figure 4.2, respectively. It was found that for this mechanism, the cycloisomerisation of pent-4-ynoic acid proceeds with lower energies overall, and a selectivity switch in favour of the 5-*anti-exo*-dig pathway was observed. The rate-determining barrier was furthermore lowered from 27.1 kcal/mol for the previous mechanism to 19.2 kcal/mol. Therefore, this mechanism with AuCl as the active catalyst is more in line with the experiments compared to the other one.

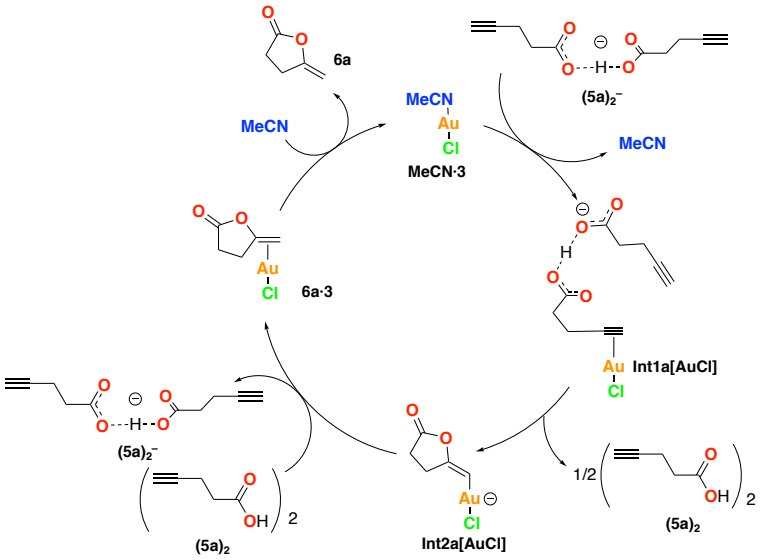

Scheme 4.4. *Catalytic cycle for the cycloisomerization of pent-4-ynoic acid by AuCl.*

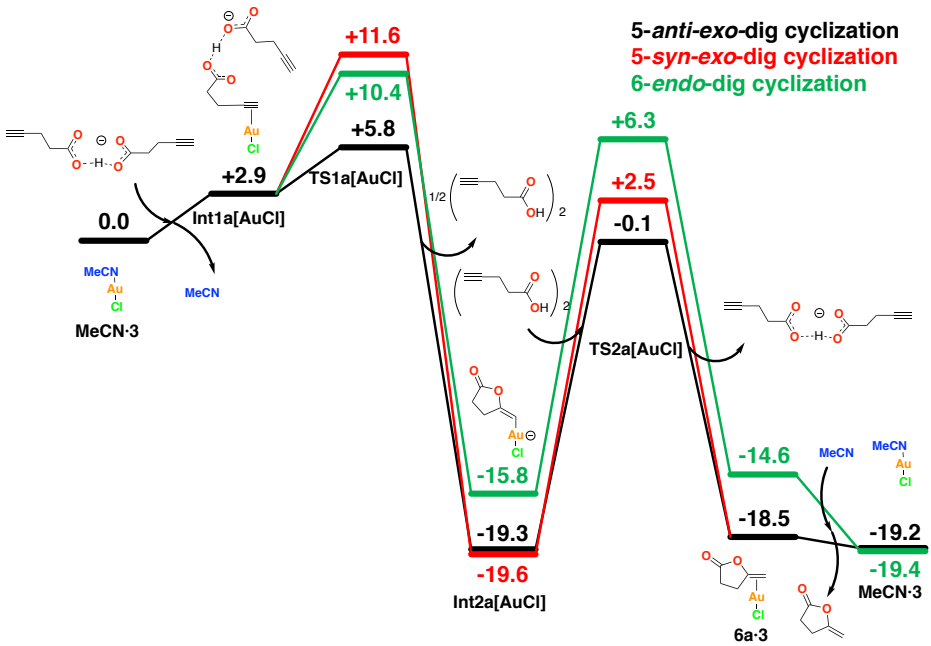

Figure 4.2. *Calculated free energy profile for the cycloisomerization of* ***1a*** *by AuCl. Energies are in kcal/mol.*

This became more apparent when the mechanism was investigated for substituted alkynes. The free energies of all intermediates and transition states are given in Table 4.2. The aforementioned bromide- and phenyl-substituted acetylenic acids **5b** and **5c** experimentally displayed full selectivity towards corresponding (*Z*)-*exo*-alkylidene γ-lactone products,[75] which was well-reproduced with this mechanism. Specifically, the 5-*exo*-dig cyclisation TSs for substrate **5b** were calculated to favour the 5-*anti*-addition by 8.3 kcal/mol. In the case of substrate **5c**, the calculations favour the 5-*anti*-addition by 7.6 kcal/mol. The mechanism shown in Scheme 4.3 could not, however, reproduce the selectivity observed experimentally for the *n*-butyl substituted substrate **5d**. Interestingly, this is the only substrate which does not follow the general selectivity towards the (*Z*)-*exo*-alkylidene γ-lactone, yielding a 1:1 mixture of the two stereoisomers instead. Instead, the calculations showed that the 5-*syn*-addition was favoured over the 5-*anti*-addition by 6.9 kcal/mol. Moreover, the 6-*endo*-dig cyclisation, whose corresponding product was not observed experimentally at all, was calculated to be the lowest-energy pathway, valued at 1.2 kcal/mol lower than the 5-*anti*-*exo*-dig cyclisation TS.

Table 4.2. *Relative energies (in kcal/mol) of intermediates and transition states for the cycloisomerization of substrates* ***5a-e*** *according to the reaction mechanism shown in Scheme 4.4. Energies are relative to* **MeCN·3**.

Substrate	Cyclization Pathway	Int1 [AuCl]	TS1 [AuCl]	Int2 [AuCl]	TS2 [AuCl]	6/7•3	Reaction energy
	5-*anti-exo*-dig		**+3.2**	-31.1	-8.8	-21.3	-26.2
5b	5-*syn-exo*-dig	+1.7	+11.5	-31.8	-5.8	-20.4	-26.1
	6-*endo*-dig		+11.5	-24.8	+0.5	-16.0	-21.9
	5-*anti-exo*-dig		**+6.5**	-17.0	+3.9	-13.9	-16.7
5c	5-*syn-exo*-dig	+1.6	+14.1	-17.4	+7.4	-13.0	-16.2
	6-*endo*-dig		+10.7	-15.1	+7.3	-12.1	-13.9
	5-*anti-exo*-dig		+9.6	-16.3	+4.5	-15.6	-15.6
5d	5-*syn-exo*-dig	+0.9	+16.5	-16.2	+8.6	-14.9	-15.5
	6-*endo*-dig		**+8.4**	-17.0	+5.7	-15.2	-15.2
	5-*anti-exo*-dig		**+5.0**	-14.7	+6.0	-14.2	-15.0
5e	5-*syn-exo*-dig	+1.3	+15.9	-14.6	+8.7	-13.7	-14.9
	6-*endo*-dig		+8.6	-15.8	+4.6	-14.1	-15.0

4.3. Conclusions

The mechanism for the cycloisomerisation of acetylenic acids catalysed by AuCl and potassium carbonate was investigated by means of DFT calculations. The calculations suggest a mechanism where AuCl is the active catalyst, without dissociation of its chloride ligand. It was found that the selectivity determining step is the cyclisation to the auro-lactone intermediate, and that the subsequent protodeauration thereof is the rate-determining step. The mechanism is consistent with the observed regio- and stereoselectivities displayed by substrates **5a-c**. However, the divergent stereoselectivity displayed experimentally by substrate **5d** cannot be explained on the basis of the current calculations.

5. Cycloisomerisation of Acetylenic Acids in Gold-Functionalised Cavitand (**Paper III**).

5.1. Introduction

As mentioned in **Chapter 1**, supramolecular hosts can exhibit catalytic potential, with many such systems designed for this purpose.[79–84] These often display unexpected reactivity patterns, and can be functionalised with transition metals.[85] This allows for the synergy of the well-established homogeneous organometallic chemistry with the confinement effects inherent to supramolecular hosts.

Resorcinarene cavitands have also experienced this functionalisation with transition metals.[16,86] One of these is a resorcin[4]arene-based cavitand with one wall functionalised with a phosphine gold chloride group (Figure 5.1).[87] This cavitand, here called **Cav-A** has demonstrated catalytic capabilities for a number of reactions,[88] most interestingly the same acetylenic acid cycloisomerisation reaction examined in **Paper II**.

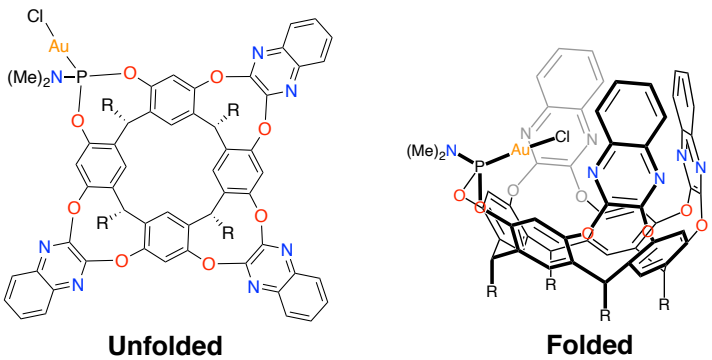

Figure 5.1. *Schematic representations of* ***Cav-A****. In the calculations, R=Me. Experimentally, R=$C_{11}H_{23}$.*

In their experiments, Ho and Schramm demonstrated that cavitand **Cav-A** is capable of cycloisomerising acetylenic acids with different substituents on the backbone, which showed interesting substrate size-dependent effects on the reactivity.[88]

To elucidate these effects on a theoretical level, DFT calculations were employed to investigate the binding and reactivity for the cycloisomerisation of acetylenic acids to lactones in cavitand **Cav-A** (Scheme 5.1). Moreover, the cycloisomerisation reaction was also investigated for a model catalyst where the cavitand walls were removed, to assess the influence of the cavitand itself on the reaction.

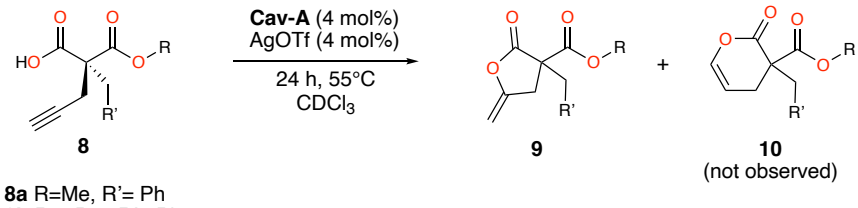

Scheme 5.1. *Cycloisomerization of acetylenic acids to their exo-methylene γ-lactones catalyzed by cavitand* ***Cav-A***.

5.2. Results and discussion

To establish an energy reference point, different host-guest complexes for cavitand **Cav-A** were examined. The possible guests include chloroform solvent molecules, the triflate counterion, acetylenic acid substrate **8a**, and combinations of these (Figure 5.2). The results show that the lowest-energy complex consists of the triflate counterion bound to the cavitand through the gold cation, with a chloroform solvent molecule occupying the remaining space on top of the cavitand (Figure 5.2). A subsequent guest exchange of the chloroform for the acetylenic acid substrate **8a** results in complex **TfO·8a⊂Cav-A**, from where the reaction takes place. The penalty for exchanging chloroform to substrate **8a** was calculated to be 4.5 kcal/mol. Exchanging both the chloroform and the triflate for substrate **8a** was associated with a penalty of 9.5 kcal/mol. These results indicate that upon introduction of a substrate, the triflate remains as a hydrogen-bond acceptor.

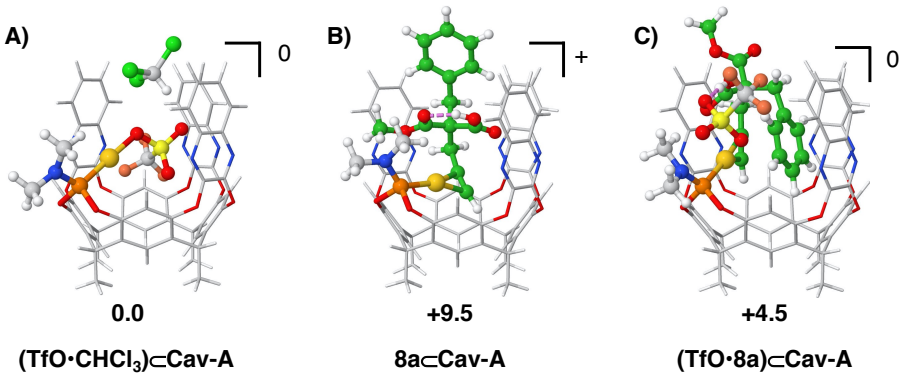

Figure 5.2. *Optimized geometries of lowest-energy conformers for possible guests in cavitand* ***Cav-A****. Relative free energies are given in kcal/mol. A) triflate and chloroform; B) Substrate* ***8a****; C) Substrate* ***8a*** *and triflate.*

The mechanism is described in Scheme 5.2, and it closely resembles the solution reaction as described in **Chapter 4**. The bound guest undergoes cyclization through either a 5-*anti-exo*-dig, 5-*syn-exo*-dig, or 6-*endo*-dig pathway. The cyclization occurs with a simultaneous proton transfer from the carboxylic acid moiety to the triflate counterion, resulting in intermediate **8a-Int$_{5anti}$⊂Cav-A** and triflic acid. The cyclisation step is both the rate- and selectivity-determining step, unlike the case for the reaction in solution. Subsequently, the triflic acid protonates the α-carbon of the intermediate to form the bound product, while regenerating the triflate counterion. A guest exchange of the product for a new substrate molecule completes the catalytic cycle.

In the case of substrate **8a**, the lowest-energy pathway is the 5-*anti-exo*-dig cyclization, with an overall barrier of 10.3 kcal/mol (Figure 5.3). This is consistent with the fact that experimentally, only the γ-lactone **9a** was observed. The 5-*syn-exo*-dig cyclization barrier is slightly higher at 11.3 kcal/mol. The 6-*endo*-dig pathway has the highest barrier, which was calculated to be 14.6 kcal/mol. In the experiments on this reaction, kinetics measurements were carried out on the cycloisomerization of **8a** catalysed by cavitand **Cav-A**. The experiments measured a rate constant of $5.59 \cdot 10^{-5}$ s^{-1} at 55°C,[88] which can be converted to a free energy barrier of 25.6 kcal/mol.

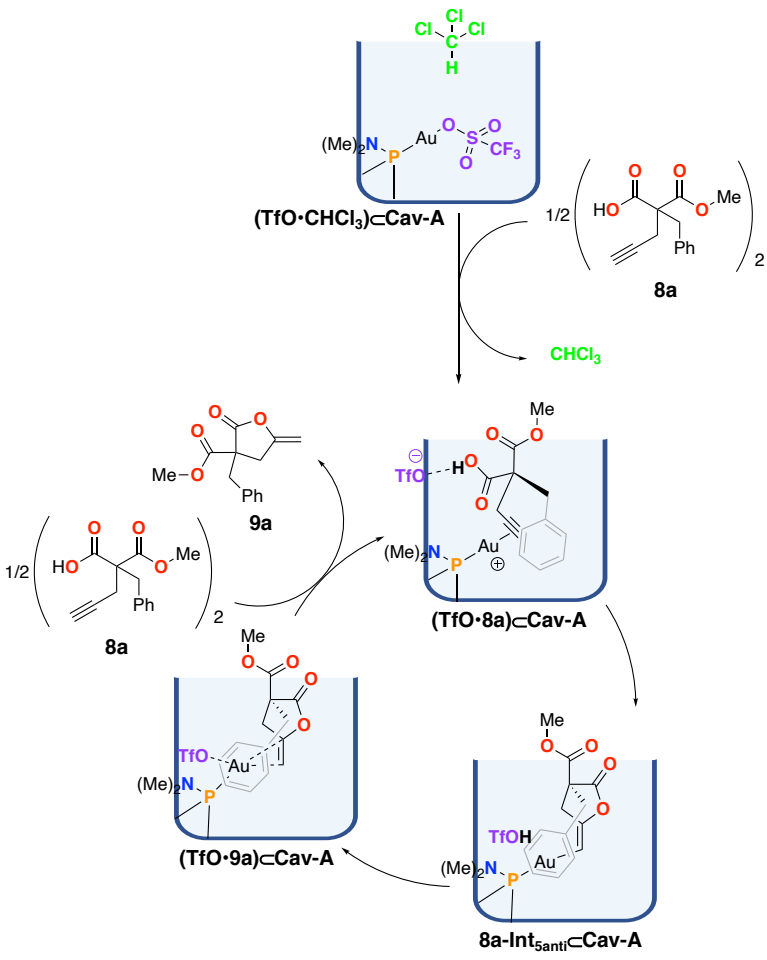

Scheme 5.2. *Catalytic cycle for the cycloisomerization of* ***8a*** *in* ***Cav-A****.*

The reason for the calculated barriers being so underestimated is not clear. One might envision that the rate-determining step is the final guest exchange, for which the energies were not calculated explicitly. This hypothesis can be dismissed due to the experimental observation that the reaction exhibits product inhibition. If it were the case that the guest exchange is the rate-determining step, adding product to the reaction mixture would not influence the rate as the equilibrium would simply be shifted forward. Instead, it is more likely that there exists a lower-energy reference point which we cannot identify.

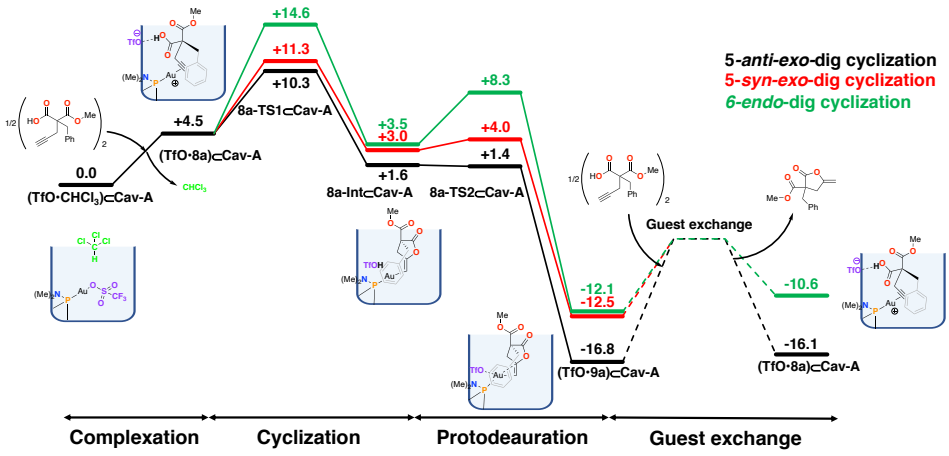

Figure 5.3. *Calculated free energy profile (kcal/mol) of the cycloisomerization of* ***8a*** *to its corresponding lactone inside cavitand* ***Cav-A****.*

Another possibility that was examined is whether the cyclization/proton transfer step might be stepwise. To that end, the 5-*anti*-*exo*-dig cyclisation TS was calculated for the cyclization of **8a** in the absence of the triflate counterion. Whilst this was calculated to be higher in energy (17.6 vs. 10.3 kcal/mol), it is still too low to reproduce the experimental rates.

To probe the effect of substitution of the ester moiety as well as the side-chain size, two other substrates were analysed. The first is substrate **8b**, where the methyl ester of substrate **8a** was replaced with a *tert*-butyl group. The second is substrate **8c**, where the benzyl substituent of substrate **8a** was replaced by a 1-naphthyl group. The results for both these substrates were similar to the ones obtained for substrate **8a**, with rate-determining steps that were likewise too low to be consistent with experimental kinetics. Notably, whilst the lowest-energy pathway for both **8a** and its *tert*-butyl ester analogue **8b** is the 5-*anti*-*exo*-dig cyclisation pathway, the 1-naphthyl substituted **8c** prefers the 5-*syn*-*exo*-dig cyclisation pathway. More importantly, it was found that whereas the concerted cyclisation/proton transfer step has a higher barrier for **8c** compared to **8a**, the opposite is true for the scenario where the cyclisation occurs without the triflate counterion present. The latter is more consistent with the experimental kinetics, which showed that **8c** reacts slightly faster compared to **8a**.

To assess the effect of the cavitand walls on the barriers of the reaction, the cavitand was simplified to dimethyl dimethylphosphoramidite, $(CH_3O)_2PN(CH_3)_2$, coordinated to a gold ion.

The cycloisomerisation of **8a** was then examined using this truncated catalyst, and the resulting free energy profiles are given in Figure 5.4.

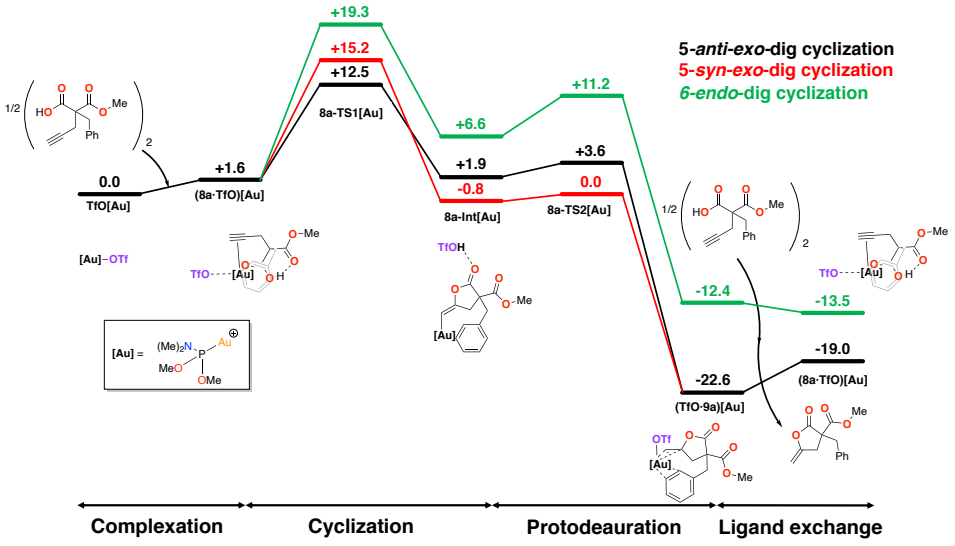

Figure 5.4. *Calculated free energy profile showing the cycloisomerization of* ***8a*** *with a truncated catalyst.*

The calculations show that the cavitand walls do provide a lowering of the rate-determining cyclisation barrier, albeit a modest one (2.2 kcal/mol). By contrast, the influence of the cavitand on the binding penalty of the substrate is more pronounced, lowering the penalty from 4.5 to 1.6 kcal/mol. Thus, whereas the overall catalytic power of the cavitand's walls is rather small, their effect on the chemical step — the cycloisomerisation reaction itself — is more significant, lowering the energy required by 5.1 kcal/mol.

5.3. Conclusions

The cycloisomerisation of acetylenic acids to their corresponding γ-lactones in a gold-functionalised resorcin[4]arene-based cavitand was investigated using DFT calculations. The calculations suggest the mechanism shown in Scheme 5.2 where, after binding a substrate molecule to the gold ion, a cyclisation step occurs followed by a protodeauration step, with the

triflate counterion acting as a proton acceptor and proton donor in these steps, respectively. A final guest exchange completes the catalytic cycle thereafter.

The rate-determining cyclisation barriers for all three substrates examined here were calculated to be too low to match experimentally measured rate constants. The selectivity of the reaction, however, is very well reproduced by the calculations, as all three substrates would exclusively form their corresponding γ-lactone products.

Lastly, the influence of the cavitand walls was examined by calculating the cycloisomerisation of **8a** by a truncated catalyst, where the cavitand walls were removed. The calculations show that, whereas the walls have a minor catalytic effect on the reaction overall, the binding penalties are increased by the cavitand. Thus, whilst the cycloisomerisation reaction itself is accelerated by cavitand **Cav-A**, the total influence is small.

6. Hydrophilic Guest Recognition in Deep Cavitand (**Paper IV**).

6.1. Introduction

As mentioned in **Chapter 1**, supramolecular cavitands have intriguing binding properties, particularly the water-soluble cavitands.[18,89–93] It has been observed experimentally that hydrophilic guests can bind very well to these hydrophobic cavitands. This is particularly interesting, since intuition would dictate that, given the choice between a hydrophobic environment and aqueous solution, hydrophilic guests would be expected to have low affinity for the hydrophobic environment. One can therefore ask how these guests bind to achieve such affinities for the cavitand.

In **Paper IV**, the recognition of a series of O-heterocyclic hydrophilic guests in a new deep cavitand **Cav-B** (Scheme 5.1) were assessed through experimental and computational means. The calculations provide a picture of the binding of these guests to the cavitand and add insight into the experimentally observed high affinity for the binding of the guests deep inside the cavitand.

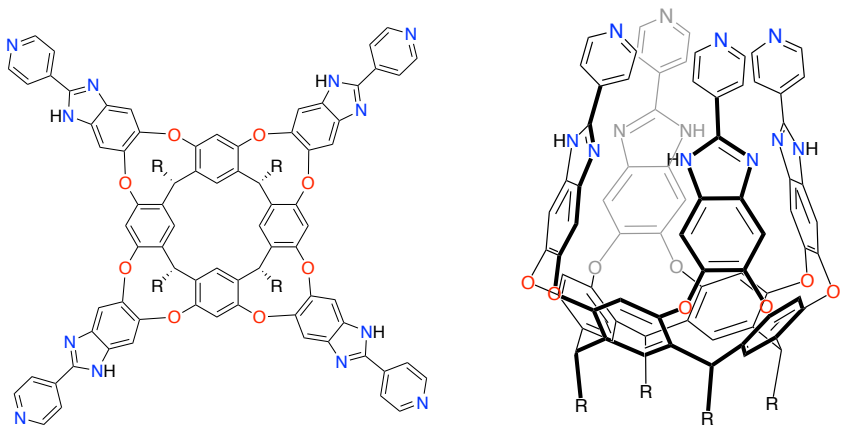

Scheme 6.1. *Schematic views of* ***Cav-B****. In the calculations, R=Me.*

6.2. Results and discussion

Calculations for host-guest models with different numbers of water molecules were carried out, and it was found that the use of twelve water molecules gives a good geometric fit. Four of the twelve water molecules are located between the panels of the cavitand, and eight inside the cavitand above the guest.

In order to shed light on the binding of the guests in the deep cavitand, the lowest-energy binding modes were calculated for a number of representative O-heterocyclic guests. These guests are THF, cyclopentanone (**CpO**), cyclopentanol (**CpOH**), 1,4-dioxane (**1,4-DO**) and 1,3-dioxane (**1,3-DO**). The most preferred binding modes are shown in Figure 6.1, and other binding modes mentioned in the text can be found in the SI of **Paper IV**. An important result is that in all cases, it was found that no hydrogen bonds can be established between the guests and the benzoimidazole moieties of the cavitand's walls.

THF was found to orient vertically in the cavitand, and receives two hydrogen bonds from water molecules in the cavitand (**THF⊂Cav-B**, Figure 6.1). These water molecules mediate between the guests and the imidazole walls of the cavitand. Other notable binding modes include ones with one hydrogen bond (+0.9 kcal/mol), no hydrogen bonds (+6.1 kcal/mol) or a hydrogen bond with a water molecule at a seam (+8.0 kcal/mol).

Cyclopentanone, on the other hand, prefers binding by accepting only one hydrogen bond from the water molecules (**CpO⊂Cav-B**). Forming a second hydrogen bond with cyclopentanone comes at an energetic penalty of 2.8 kcal/mol. Conformers with no hydrogen bonds are more than 3.3 kcal/mol higher than the lowest-energy conformer.

The case of cyclopentanol is special, since this is the only guest studied here that can donate hydrogen bonds as well as accept them. However, the lowest calculated conformer has cyclopentanol accepting one hydrogen bond without donating any (**CpOH⊂Cav-B**). The lowest conformer where cyclopentanol donates a hydrogen bond was found to be only 0.9 kcal/mol higher.

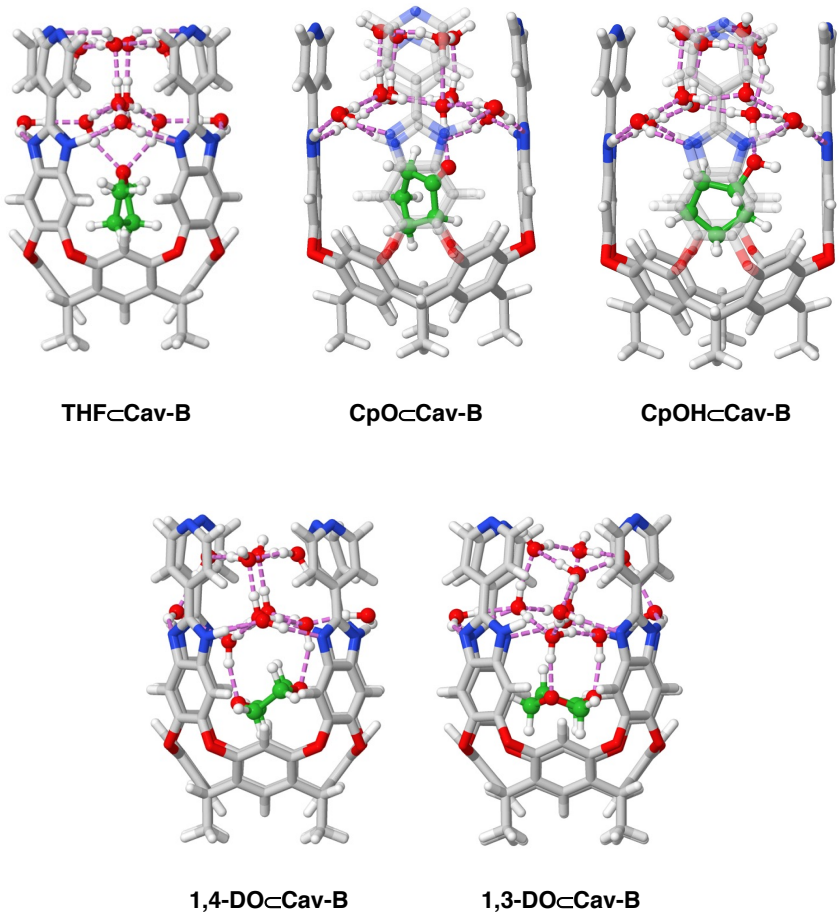

Figure 6.1. *Optimised structures of guests bound to* ***Cav-B****. From left to right: THF, cyclopentanone, cyclopentanol, 1,4-dioxane and 1,3-dioxane.*

1,4-dioxane has two oxygen atoms, both capable of receiving hydrogen bonds. This guest has several conformers with only minor energy differences (≤1 kcal/mol). Two of these are isoenergetic. The first involves the horizontally oriented dioxane receiving one hydrogen bond, while the second is a horizontally oriented dioxane with two hydrogen bonds (**1,4-DO⊂Cav-B**). Two other conformers were found with low energies. One is the vertically oriented dioxane receiving one hydrogen bond (+0.5 kcal/mol), while the other is a similarly oriented dioxane with two hydrogen bonds at the same oxygen atom (+0.6 kcal/mol). The small difference

between the horizontal and vertical orientations of the guest in the cavitand is in line with NMR data showing a single signal for 1,4-dioxane due to rapid spinning or flipping.

Similar to 1,4-dioxane, 1,3-dioxane has three conformers within 1 kcal/mol from the lowest-energy one. This lowest-lying conformer involves a horizontally oriented guest accepting two hydrogen bonds from two adjacent water molecules (**1,3-DO⊂Cav-B**). It should be noted that the guest lies deep in the cavitand in this conformer, in line with larger observed upfield NMR signal shifts for 1,3-dioxane compared to 1,4-dioxane. The vertically oriented counterpart of the aforementioned conformer is 0.2 kcal/mol higher in energy. A vertically oriented 1,3-dioxane with two hydrogen bonds from non-adjacent water molecules has a relative free energy of +1.0 kcal/mol compared to the lowest-energy conformer.

Non-covalent interaction (NCI) analysis was employed to elucidate the nature of the binding of guests inside the cavitand, with THF as a representative guest (Figure 6.2). The analysis was performed on a host-guest systems with zero and twelve water molecules. In the absence of water molecules (Figure 6.2, left), the cavitand and THF interact through weak dispersion interactions. Upon inclusion of water molecules, the guest forms additional favourable hydrogen bonds with the water molecules (Figure 6.2, middle). The water molecules at the seams interact with the cavitand through hydrogen bonds between the pyridinyl-benzimidazole panels, and through dispersion interactions at the upper half of the cavitand (Figure 6.2, right).

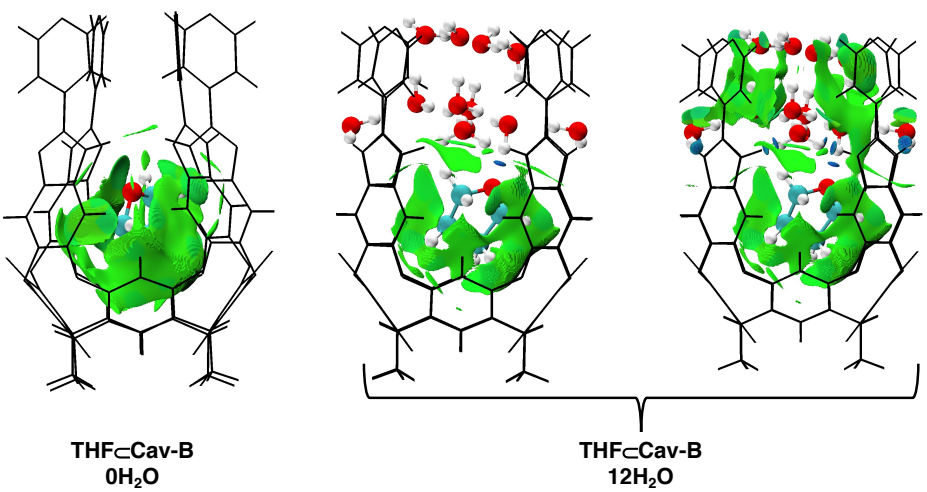

Figure 6.2. *NCI analysis of THF in* ***Cav-B****. For clarity, the middle only shows intramolecular interactions involving the guest, while on the right all interactions are displayed.*

6.3. Conclusions

The calculations provide a picture of how the hydrophilic guests studied here bind to a deep, water-soluble cavitand. The guests were found to bind to the cavitand through hydrogen bonds with water molecules higher in the cavitand. These water molecules in turn form hydrogen bonding networks with the cavitand.

7. Hydrolysis of Acetylcholine in Resorcinarene-Based Cavitand (**Paper V**).

7.1. Introduction

As a greener alternative to organic solvents, water is becoming an increasingly desirable solvent for chemical reactions.[94–96] However, many organic reagents are insoluble in aqueous solution. Additionally, the strong interactions from water can sometimes hinder the reaction.

To overcome this issue, supramolecular host-guest complexes offer a solution. The interior of resorcin[4]arene cavitands provides a hydrophobic microenvironment, and modifications to the feet of the cavitand through a saponification reaction can make them water-soluble. These water-soluble cavitands have demonstrated catalytic capabilities for a number of reactions in the past.[97–101]

Cavitand **Cav-C** (Scheme 7.1) is capable of binding molecules of complementary sizes, with its hydrophilic rim featuring urea-type panels that provide many hydrogen bond acceptor/donor sites. However, little is known about the cavitand's capabilities in terms of reactivity. One interesting hypothesis is that the large preorganisation of water molecules through hydrogen-bonding may provide enough catalytic power to potentially lower reaction barriers.

To test this hypothesis, we present DFT calculations on the hydrolysis of an ester in cavitand **Cav-C** to determine whether the cavitand possesses catalytic power. Acetylcholine (**11**) was chosen as a model guest for this reaction because of its appropriate size for binding to **Cav-C**, and because it is an important ester with biological applications as a key neuromodulator for several important neurological processes.[102–105]

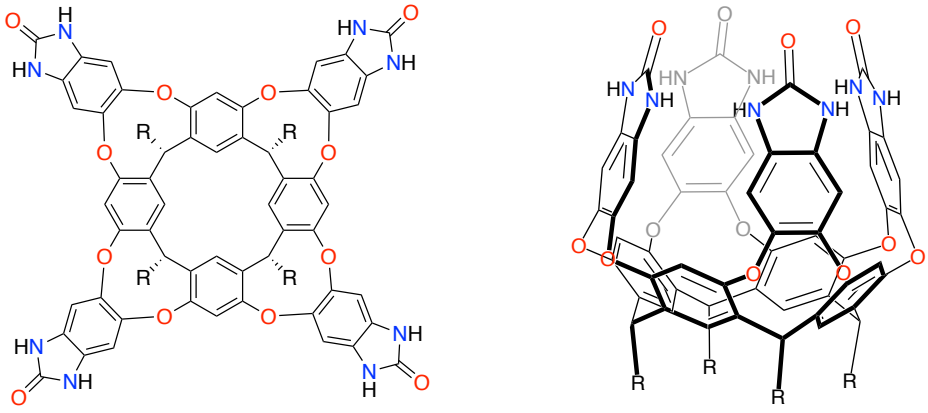

Scheme 7.1. *Schematic views of* ***Cav-C****. In the calculations, R=Me.*

7.2. Results and Discussion

Before examining the hydrolysis reaction in cavitand **Cav-C**, it is important to consider the reaction in bulk solution. The neutral ester hydrolysis reaction proceeds through a two-step addition-elimination mechanism as depicted in Scheme 7.2.

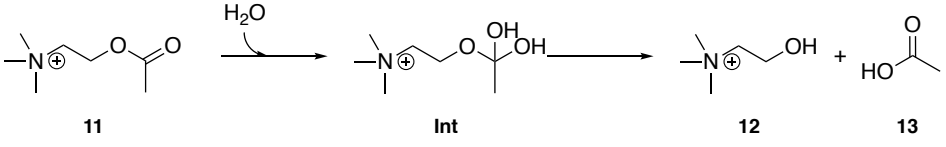

Scheme 7.2. *Mechanism of neutral hydrolysis of acetylcholine*

In the addition step, a nucleophilic addition of OH^- and a protonation of the acyl oxygen take place in a single concerted step, leading to a *gem*-diol intermediate. The C-O bond is then cleaved during the elimination step, accompanied by a proton transfer from one of the alcohol groups to the alkoxy leaving group. This elimination results in the formation of the products, acetic acid and choline. The free energy profile for this reaction is given in Figure 7.1. The addition step is the rate-determining step, and both steps can be facilitated through proton shuttles via cyclic transition states. The calculations showed that the use of two water molecules as proton shuttles in both steps resulted in barriers consistent with experimental kinetics. The

computed free energy barrier for the reaction was 32.6 kcal/mol, in reasonable agreement with the measured barrier for this step, 28.5 kcal/mol.[106]

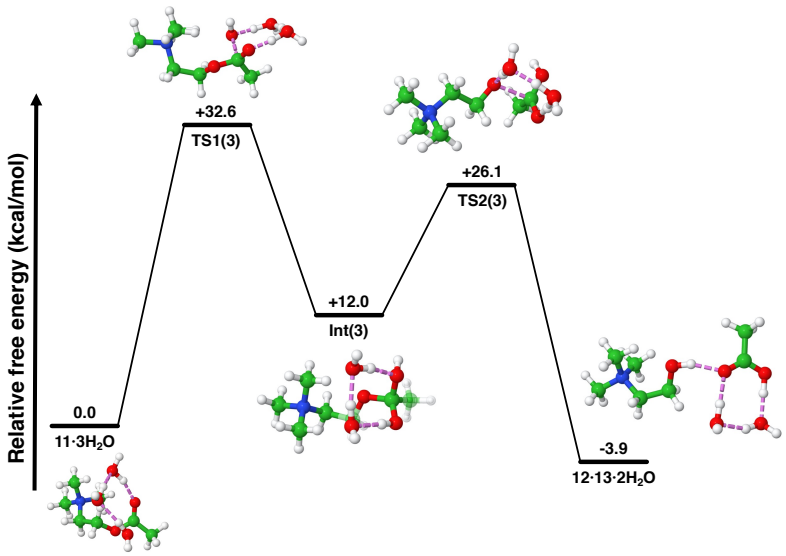

Figure 7.1. *Free energy profile for the hydrolysis of* ***11*** *in solution.*

The calculations showed that acetylcholine binds to **Cav-C** in a coiled conformation, with the trimethylammonium moiety at the bottom and the acetyl group located near the rim (Figure 7.2). Additionally, it was found that twelve water molecules orient themselves in three layers, as shown in Figure 7.2.

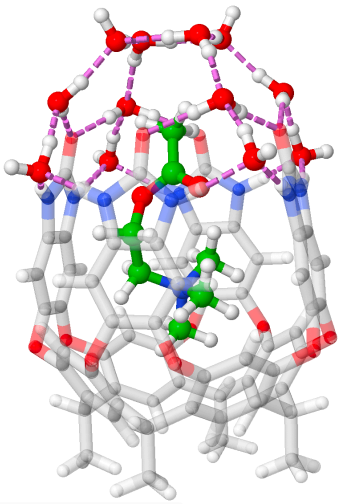

Figure 7.2. *Optimised geometry of the lowest-energy binding mode of* ***11⊂Cav-C****.*

The free energy profiles for the neutral hydrolysis of acetylcholine are given in Figure 7.3., comparing the reaction in solution (red) with the reaction in cavitand **Cav-C** (black). The calculations show that the cavitand does not impact the energy of the addition step, as the barrier was found to be almost identical to the solution case. By contrast, the subsequent elimination step was calculated to be much higher than its analogue in solution. This effect arises because, in the hydrophobic cavity, the proton transfer step requires a water molecule to diffuse deep into the cavitand in order to complete the proton transfer following cleavage of the alkoxy bond. The hydrophobic cavity disfavours this transfer, resulting in a much higher barrier.

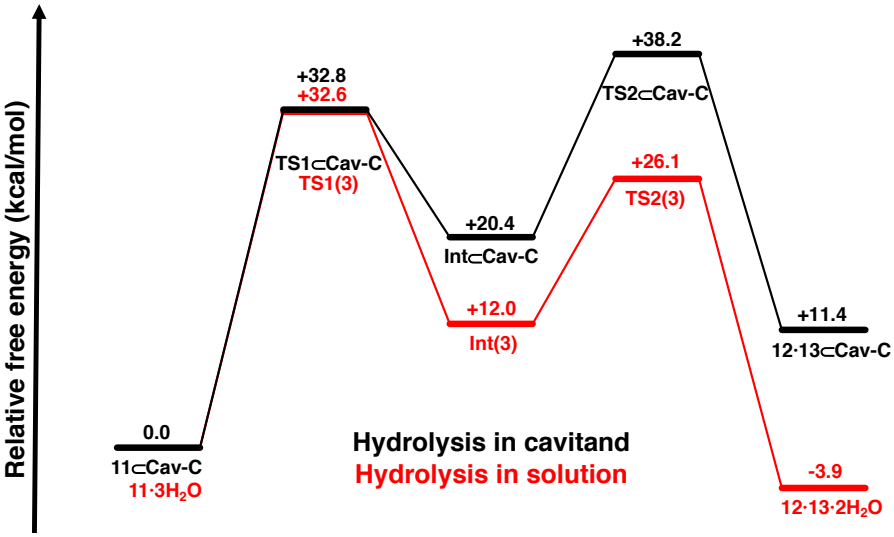

Figure 7.3. *Calculated free energy profiles for the hydrolysis of acetylcholine in a cavitand and in solution.*

7.3. Conclusions

The mechanism for the hydrolysis of acetylcholine was investigated both in aqueous solution and in the presence of a resorcinarene-based cavitand using DFT calculations. The influence of the cavitand was assessed by comparing the free energy profiles of the hydrolysis reaction in both environments. The calculations show that cavitand **Cav-C** does not exhibit

catalytic power for ester hydrolysis. While it has minimal influence on the addition step, it raises the barrier for the elimination step significantly due to the difficulty of the proton transfer in the hydrophobic cavity. As such, the cavitand hinders this reaction, ruling it out as a potential catalyst for ester hydrolysis.

8. Concluding remarks

In this thesis, density functional theory calculations were employed to study a number of chemical systems. Two of these are homogeneous organometallic catalytic reactions (**Paper I** and **Paper II**) and three others pertain to supramolecular chemistry (**Papers III-V**). The employment of QM methods allowed for the elucidation of many details for each chemical system.

As a good example of the synergy that can be achieved between experimental and computational techniques, the reaction mechanism of the dehydrogenation of amines using (cyclopentadienone)iron carbonyl catalysts was studied (**Paper I**). Kinetic isotope effect studies strongly suggested a stepwise mechanism involving a rate-determining C-H cleavage and a fast proton transfer. These observations were corroborated by DFT calculations, suggesting a reaction mechanism starting from an iron-amine adduct. Such a complex was isolated and characterised by NMR analysis and X-ray crystallography. From the iron-amine adduct, a coordination change occurs from the nitrogen atom to a hydride atom. That hydride will subsequently be transferred from the amine substrate to the metal, resulting in an iminium-metal hydride ion pair. A proton transfer then occurs from the iminium ion to the cyclopentadienone ligand, yielding the final products. The results are consistent the experimental results as well as with computational studies in the literature.

DFT was also used to model the full mechanism for the cycloisomerisation of acetylenic acids catalysed by gold(I) chloride into lactones (**Paper II**). It was found that the selectivity-determining cyclisation preferably occurs via an 5-*anti*-*exo*-dig cyclisation, making it highly regioselective towards γ-alkylidene lactones, and highly stereoselective towards the (*Z*)-steroisomer products, which is in line with the experimentally observed regio- and stereoselectivities for substituted acetylenic acids. However, the calculations cannot explain the one exception to this rule in the case of an *n*-butyl substituted alkyne acid.

The same cycloisomerisation reaction was also studied in a gold-functionalised resorcin[4]arene cavitand (**Paper III**). Three substrates with different substitution patterns were examined as representative examples for the influence of substrate size on the reactivity. The mechanism is analogous to the reaction in solution, where after an initial guest exchange for an acetylenic acid, a combined cyclisation/proton transfer takes place, followed by a

protodeauration to yield the enol-lactone products. Whereas the selectivity towards γ-lactones is well-reproduced in the calculations, the computed total barriers for all three substrates were too low to match the experimental kinetic data. The influence of the cavitand structure on the reactivity was elucidated by calculating the cycloisomerisation of one substrate by a truncated catalyst, where the cavitand walls and bottom were removed. These calculations showed that the cavitand raises the binding penalty for the substrate, but also lowers the energy required for the cyclisation to take place thereafter. These two observations result in a modest catalytic effect of the cavitand.

The recognition of small hydrophilic guests in a newly developed deep, water-soluble, resorcin[4]arene cavitand with pyridinyl-benzimidazole walls was studied (**Paper IV**). Water molecules interact with the cavitand by forming hydrogen bonds with the panels at the seams. The guests bind in the cavitand with dispersion forces at the bottom of the cavitand, and form water-mediated hydrogen bonds with the cavitand. Conformational analysis of the binding modes of the guests with the cavitand was carried out for THF, cyclopentanone, cyclopentanol, 1,3-dioxane and 1,4-dioxane. The analysis concurs with experimental data for the binding of these guests.

Lastly, a mechanistic study was conducted to examine the possibility for a water-soluble resorcin[4]arene cavitand to catalyse the hydrolysis of acetylcholine (**Paper V**). The hydrolysis of acetylcholine in solution was studied first, and a two-step addition-elimination mechanism was calculated. A cavitand model with twelve water molecules was used, and the resulting energy profile gave a prohibitively high barrier for the elimination step, whereas the addition step has a very similar barrier as in solution. As a result, it was concluded that the cavitand cannot catalyse the hydrolysis reaction.

The calculations presented in this thesis demonstrate the power of DFT calculations in unravelling reaction mechanisms in both homogeneous organometallic catalysis and supramolecular chemistry. It is evident that calculations will continue to play a major role in research in chemistry in the future, in the capacity as a corrector, a clarifier, and as a predictor.

9. Acknowledgements

This is the culmination of four and a half years' work, as well as (hopefully) the last time I write a thesis. But of course, I was not alone in creating everything here. Over the years, I have enjoyed the help and support of many people and as such, it is only right that I acknowledge everyone who helped make this possible.

First of all, I would like to thank my advisor, *Prof. Dr. Fahmi Himo*, for granting me the opportunity to pursue a PhD under his guidance. I thank you for all your expertise, support and good humour over the years. May your chess score ever increase.

The same gratitude is extended to my co-supervisor and the current Director of Doctoral Studies, *Prof. Dr. Kalman Szabó*, and to *Prof. Dr. Joseph Samec*, for proofreading this thesis.

And to the former Director of Doctoral Studies, *Prof. Dr. Belén Martín-Matute*, I thank you for your valuable feedback and support for the halftime report. It most certainly made writing the second half much faster.

I would also like to thank all of collaborators in all works presented here: *Prof. Dr. Julius Rebek Jr.*, *Prof. Dr. Yang Yu*, *Prof. Dr. Jan-Erling Bäckvall*, *Dr. Srimanta Manna*, *Dr. Aitor Bermejo-Lopez*, *Dr. Oriana Brea*, *Dr. Hua-Wei Guan* and *Dr. Yu-Jie Zhu*.

To all current and former members of the Himo group, as well as the long-term visitors I had the pleasure of meeting: *Prof. Dr. Xiang Sheng*, *Dr. Wen-Jie Wei*, *Dr. Akinobu Matsuzawa*, *Dr. Man Li*, *Dr. Oriana Brea*, *Dr. Ferran Planas*, *Dr. Mario Prejanó*, *Dr. Maria Biosca*, *Dr. Gantulga Norjmaa*, *Dr. Jia-yi Chen*, *Dr. Francesco Calcagno*, *Dr. Shuo-Qi Sun*, *Dr. Shi-Qing Zhou*, and *Prof. Dr. Yuta Hori*. I have watched you all come and go, but I have never forgotten you. For all your feedback on my science, for all your companionship, and for your help throughout the years, I thank you. To *Lukas Römer*: your journey has just begun, but I already know you will succeed. Take good care of Celsius and Kelvin, they're your best friends here now. And thanks for being a good office mate.

Not to be forgotten are the group visitors whom I had the pleasure of teaching computational chemistry: *Quentin Joachim*, *Dr. Maria Victoria Lopez Corbalan, Marc Rüttiman*, *Emil Mossberg*, and *Pernilla Öberg*. I enjoyed teaching all of you much more than I showed.

Furthermore, I thank all my colleagues in the organic chemistry unit, both present and former, who make coming to work a pleasurable experience. Your companionship truly is the

greatest part of working here. Among those not already mentioned, I thank *Tautvydas*, *Denise*, *Michael*, *Sybrand*, *Linus*, *Marie*, *Kevin* (KS Group), *Zainab*, *Ylva*, *Tanguy*, *Astrid*, *Stefanie*, *Beatriz* (AM Group), *Beatriz* (BMM Group), *Matteo*, *Emanuele*, *Ha*, *Alexandru*, *Pedro*, *Alba*, *Majken*, *Pamela*, *Pol*, *Niki*, *Biswanath*, *Björn*, *Ivo*, *Bram*, *Luca*, *Norman*, *Tomasso*, *Michail*, *Haibo*, *Gonzalo*, *Kevin* (GW Group), *Miguel*, *Spandan*, *Anson*, *Paul*, *Leonie*, *Berit*, *Ester*, *Leonard*, *Benjamin*, *Judith*, *Erika*, *Miguel*, *Sayad*, *Daria*, *Igor*, *Dear*, *Jedi*, *Davide*, *Shida*, *Afroditi*, *William* and *Lala*.

It is rarely acknowledged how much the department's administrators and technicians mean for the researchers. Whether it is filing travel expense reports, inquiries into rules and regulations, or solving technical issues which we cannot deal with ourselves. For that, I thank the many administrators we have had over the years: *Sigrid*, *Petra*, *Mattias*, *Gabriella*, *Martin* and *Kristina*. Above all, I thank *Ola Andersson*, our IT technician, for all the help with the servers and computers over the last five years.

Als laatste wil ik mijn eigen familie bedanken. Mijn broers *Bas* en *Luc*, mijn ouders *Marie-José* en *Jos,* en mijn grootouders *Bennie & Eddie*. Jullie hebben mij door de jaren heen gesteund. Door mijn successen, door mijn mislukkingen, door mijn blijheid, en door mijn verdriet. Niet alleen deze laatste jaren, maar altijd. En daarom kan ik hier en nu zeggen dat ik hartstikke trots ben om jullie allemaal mijn familie te noemen.

Circa 8000 calculations were made for this thesis.

10. References

(1) Chaves, J. O.; de Souza, M. C.; da Silva, L. C.; Lachos-Perez, D.; Torres-Mayanga, P. C.; Machado, A. P. da F.; Forster-Carneiro, T.; Vázquez-Espinosa, M.; González-de-Peredo, A. V.; Barbero, G. F.; Rostagno, M. A. Extraction of Flavonoids From Natural Sources Using Modern Techniques. *Front Chem* **2020**, *8*, 507887.

(2) Simonet, B. M.; Valcárcel, M. Analytical Chemistry in Modern Society: What We Can Expect. *Microchimica Acta* **2006**, *153* (1–2), 1–5.

(3) Sperger, T.; Sanhueza, I. A.; Schoenebeck, F. Computation and Experiment: A Powerful Combination to Understand and Predict Reactivities. *Acc Chem Res* **2016**, *49* (6), 1311–1319.

(4) Lan, J.; Li, X.; Yang, Y.; Zhang, X.; Chung, L. W. New Insights and Predictions into Complex Homogeneous Reactions Enabled by Computational Chemistry in Synergy with Experiments: Isotopes and Mechanisms. *Acc Chem Res* **2022**, *55* (8), 1109–1123.

(5) Becke, A. D. Perspective: Fifty Years of Density-Functional Theory in Chemical Physics. *J Chem Phys* **2014**, *140* (18), 18A301.

(6) Franco, F.; Rettenmaier, C.; Jeon, H. S.; Roldan Cuenya, B. Transition Metal-Based Catalysts for the Electrochemical CO2reduction: From Atoms and Molecules to Nanostructured Materials. *Chem Soc Rev* **2020**, *49* (19), 6884–6946.

(7) Han, Y. F.; Jin, G. X. Half-Sandwich Iridium- and Rhodium-Based Organometallic Architectures: Rational Design, Synthesis, Characterization, and Applications. *Acc Chem Res* **2014**, *47* (12), 3571–3579.

(8) Deuss, P. J.; Barta, K.; De Vries, J. G. Homogeneous Catalysis for the Conversion of Biomass and Biomass-Derived Platform Chemicals. *Catal Sci Technol* **2014**, *4* (5), 1174–1196.

(9) Chavez, F. A.; Mascharak, P. K. Co(III) - Alkylperoxo Complexes: Syntheses, Structure - Reactivity Correlations, and Use in the Oxidation of Hydrocarbons. *Acc Chem Res* **2000**, *33* (8), 539–545.

(10) Lan, J.; Li, X.; Yang, Y.; Zhang, X.; Chung, L. W. New Insights and Predictions into Complex Homogeneous Reactions Enabled by Computational Chemistry in Synergy with Experiments: Isotopes and Mechanisms. *Acc Chem Res* **2022**, *55* (8), 1109–1123.

(11) Sperger, T.; Sanhueza, I. A.; Kalvet, I.; Schoenebeck, F. Computational Studies of Synthetically Relevant Homogeneous Organometallic Catalysis Involving Ni, Pd, Ir, and Rh: An Overview of Commonly Employed DFT Methods and Mechanistic Insights. *Chem Rev* **2015**, *115* (17), 9532–9586.

(12) Grommet, A. B.; Feller, M.; Klajn, R. Chemical Reactivity under Nanoconfinement. *Nat Nanotechnol* **2020**, *15* (4), 256–271.

(13) Mouarrawis, V.; Plessius, R.; van der Vlugt, J. I.; Reek, J. N. H. Confinement Effects in Catalysis Using Well-Defined Materials and Cages. *Front Chem* **2018**, *6*, 623.

(14) Ballester, P.; Vidal-Ferran, A.; van Leeuwen, P. W. N. M. Modern Strategies in Supramolecular Catalysis. In *Advances in Catalysis*; 2011; Vol. 54, pp 63–126.

(15) Gaeta, C.; La Manna, P.; De Rosa, M.; Soriente, A.; Talotta, C.; Neri, P. Supramolecular Catalysis with Self-Assembled Capsules and Cages: What Happens in Confined Spaces. *ChemCatChem* **2021**, *13* (7), 1638–1658.

(16) Natarajan, N.; Brenner, E.; Sémeril, D.; Matt, D.; Harrowfield, J. The Use of Resorcinarene Cavitands in Metal-Based Catalysis. *Eur J Org Chem* **2017**, *2017* (41), 6100–6113.

(17) Murray, J.; Kim, K.; Ogoshi, T.; Yao, W.; Gibb, B. C. The Aqueous Supramolecular Chemistry of Cucurbit[n]Urils, Pillar[n]Arenes and Deep-Cavity Cavitands. *Chem Soc Rev* **2017**, *46* (9), 2479–2496.

(18) Biros, S. M.; Rebek, J. Structure and Binding Properties of Water-Soluble Cavitands and Capsules. *Chem Soc Rev* **2007**, *36* (1), 93–104.

(19) Oshovsky, G. V.; Reinhoudt, D. N.; Verboom, W. Supramolecular Chemistry in Water. *Angew Chem Int Ed* **2007**, *46* (14), 2366–2393.

(20) Koch, Wolfram.; Holthausen, M. C. *A Chemist's Guide to Density Functional Theory*; Wiley-VCH, 2001.

(21) Hohenberg, P.; Kohn, W. Inhomogeneous Electron Gas. *Phys Rev* **1964**, *136* (3B), 864–871.

(22) Kohn, W.; Sham, L. J. Self-Consistent Equations Including Exchange and Correlation Effects*. *Phys Rev* **1965**, *140* (4A), 1133–1138.

(23) Becke, A. D. Density-Functional Thermochemistry. III. The Role of Exact Exchange. *J Chem Phys* **1993**, *98* (7), 5648–5652.

(24) Lee, C.; Yang, W.; Parr, R. G. Development of the Colle-Salvetti Correlation-Energy Formula into a Functional of the Electron Density. *Phys Rev B* **1988**, *37*, 785–789.

(25) Grimme, S. Density Functional Theory with London Dispersion Corrections. *WIREs* **2011**, *1* (2), 211–228.

(26) Grimme, S.; Antony, J.; Ehrlich, S.; Krieg, H. A Consistent and Accurate Ab Initio Parametrization of Density Functional Dispersion Correction (DFT-D) for the 94 Elements H-Pu. *J Chem Phys* **2010**, *132* (15), 154104.

(27) Grimme, S.; Ehrlich, S.; Goerigk, L. Effect of the Damping Function in Dispersion Corrected Density Functional Theory. *J Comput Chem* **2011**, *32* (7), 1456–1465.

(28) Ochterski, J. W. *Thermochemistry in Gaussian*; 2000.

(29) Jensen, F. Statistical Mechanics and Transition State Theory. In *Introduction to Computational Chemistry*. Wiley-VCH, Weinheim, 2007, pp 421-444.

(30) Grimme, S. Supramolecular Binding Thermodynamics by Dispersion-Corrected Density Functional Theory. *Chem Eur J* **2012**, *18* (32), 9955–9964.

(31) Frisch, M. J.; Trucks, G. W.; Schlegel, H. B.; Scuseria, G. E.; Robb, M. A.; Cheeseman, J. R.; Scalmani, G.; Barone, V.; Petersson, G. A.; Nakatsuji, H.; Li, X.; Caricato, M.; Marenich, A. V.; Bloino, J.; Janesko, B. G.; Gomperts, R.; Mennucci, B.; Hratchian, H. P.; Ortiz, J. V.; Izmaylov, A. F.; Sonnenberg, J. L.; Williams-Young, D.; Ding, F.; Lipparini, F.; Egidi, F.; Goings, J.; Peng, B.; Petrone, A.; Henderson, T.; Ranasinghe, D.; Zakrzewski, V. G.; Gao, J.; Rega, N.; Zheng, G.; Liang, W.; Hada, M.; Ehara, M.; Toyota, K.; Fukuda, R.; Hasegawa, J.; Ishida, M.; Nakajima, T.; Honda, Y.; Kitao, O.; Nakai, H.; Vreven, T.; Throssell, K.; Montgomery, J. A. , Jr.; Peralta, J. E.; Ogliaro, F.; Bearpark, M. J.; Heyd, J. J.; Brothers, E. N.; Kudin, K. N.; Staroverov, V. N.; Keith, T. A.; Kobayashi, R.; Normand, J.; Raghavachari, K.; Rendell, A. P.; Burant, J. C.; Iyengar, S. S.; Tomasi, J.; Cossi, M.; Millam, J. M.; Klene, M.; Adamo, C.; Cammi, R.; Ochterski, J. W.; Martin, R. L.; Morokuma, K.; Farkas, O.; Foresman, J. B.; Fox, D. J. Gaussian16, Revision C.01. *Gaussian, Inc., Wallingford CT,*. 2016.

(32) Marenich, A. V.; Cramer, C. J.; Truhlar, D. G. Universal Solvation Model Based on Solute Electron Density and on a Continuum Model of the Solvent Defined by the Bulk Dielectric Constant and Atomic Surface Tensions. *J Phys Chem B* **2009**, *113* (18), 6378–6396.

(33) Johnson, E. R.; Keinan, S.; Mori-Sánchez, P.; Contreras-García, J.; Cohen, A. J.; Yang, W. Revealing Noncovalent Interactions. *J Am Chem Soc* **2010**, *132* (18), 6498–6506.

(34) Crabtree, R. H. Homogeneous Transition Metal Catalysis of Acceptorless Dehydrogenative Alcohol Oxidation: Applications in Hydrogen Storage and to Heterocycle Synthesis. *Chem Rev* **2017**, *117* (13), 9228–9246.

(35) Zell, T.; Milstein, D. Hydrogenation and Dehydrogenation Iron Pincer Catalysts Capable of Metal-Ligand Cooperation by Aromatization/Dearomatization. *Acc Chem Res* **2015**, *48* (7), 1979–1994.

(36) Thai, T. T.; Mérel, D. S.; Poater, A.; Gaillard, S.; Renaud, J. L. Highly Active Phosphine-Free Bifunctional Iron Complex for Hydrogenation of Bicarbonate and Reductive Amination. *Chem Eur J* **2015**, *21* (19), 7066–7070.

(37) Filonenko, G. A.; Van Putten, R.; Hensen, E. J. M.; Pidko, E. A. Catalytic (de)Hydrogenation Promoted by Non-Precious Metals-Co, Fe and Mn: Recent Advances in an Emerging Field. *Chem Soc Rev* **2018**, *47* (4), 1459–1483.

(38) Reppe, W.; Vetter, I. Carbonylierung VI Synthesen Mit Metallcarbonylwasserstoffen. *Justus Liebis Ann Chem* **1953**, *582* (1), 133–161.

(39) Knölker, H. J.; Goesmann, H.; Klauss, R. A Novel Method for the Demetalation of Tricarbonyliron - Diene Complexes by a Photolytically Induced Ligand Exchange Reaction with Acetonitrile. *Angew Chem Int Ed* **1999**, *38* (5), 702–705.

(40) Funk, T. W.; Mahoney, A. R.; Sponenburg, R. A.; Zimmerman, K. P.; Kim, D. K.; Harrison, E. E. Synthesis and Catalytic Activity of (3,4-Diphenylcyclopentadienone)Iron Tricarbonyl Compounds in Transfer Hydrogenations and Dehydrogenations. *Organometallics* **2018**, *37* (7), 1133–1140.

(41) Casey, C. P.; Guan, H. An Efficient and Chemoselective Iron Catalyst for the Hydrogenation of Ketones. *J Am Chem Soc* **2007**, *129* (18), 5816–5817.

(42) Casey, C. P.; Guan, H. Cyclopentadienone Iron Alcohol Complexes: Synthesis, Reactivity, and Implications for the Mechanism of Iron-Catalyzed Hydrogenation of Aldehydes. *J Am Chem Soc* **2009**, *131* (7), 2499–2507.

(43) Akter, M.; Anbarasan, P. (Cyclopentadienone)Iron Complexes: Synthesis, Mechanism and Applications in Organic Synthesis. *Chem Asian J* **2021**, *16* (13), 1703–1724.

(44) vonderHöh, A.; Berkessel, A. Insight into the Mechanism of Dihydrogen-Heterolysis at Cyclopentadienone Iron Complexes and Subsequent C, X Hydrogenation. *ChemCatChem* **2011**, *3* (5), 861–867.

(45) Seck, C.; Mbaye, M. D.; Coufourier, S.; Lator, A.; Lohier, J. F.; Poater, A.; Ward, T. R.; Gaillard, S.; Renaud, J. L. Alkylation of Ketones Catalyzed by Bifunctional Iron Complexes: From Mechanistic Understanding to Application. *ChemCatChem* **2017**, *9* (23), 4410–4416.

(46) Thai, T. T.; Mérel, D. S.; Poater, A.; Gaillard, S.; Renaud, J. L. Highly Active Phosphine-Free Bifunctional Iron Complex for Hydrogenation of Bicarbonate and Reductive Amination. *Chem Eur J* **2015**, *21* (19), 7066–7070.

(47) Moulin, S.; Dentel, H.; Pagnoux-Ozherelyeva, A.; Gaillard, S.; Poater, A.; Cavallo, L.; Lohier, J. F.; Renaud, J. L. Bifunctional (Cyclopentadienone)Iron-Tricarbonyl Complexes: Synthesis,

Computational Studies and Application in Reductive Amination. *Chem Eur J* **2013**, *19* (52), 17881–17890.

(48) Gimferrer, M.; Joly, N.; Escayola, S.; Viñas, E.; Gaillard, S.; Solà, M.; Renaud, J. L.; Salvador, P.; Poater, A. Knölker Iron Catalysts for Hydrogenation Revisited: A Nonspectator Solvent and Fine-Tuning. *Organometallics* **2022**.

(49) Brenna, D.; Rossi, S.; Cozzi, F.; Benaglia, M. Iron Catalyzed Diastereoselective Hydrogenation of Chiral Imines. *Org Biomol Chem* **2017**, *15* (27), 5685–5688.

(50) Hopmann, K. H. Iron/Brønsted Acid Catalyzed Asymmetric Hydrogenation: Mechanism and Selectivity-Determining Interactions. *Chem Eur J* **2015**, *21* (28), 10020–10030.

(51) Lu, X.; Zhang, Y.; Zhang, M.; Li, T. The Effect of Substituents on the Hydrogenation of an Aldehyde Catalyzed by Knölker's Catalyst. *J Organomet Chem* **2014**, *749*, 69–74.

(52) Ge, H.; Chen, X.; Yang, X. Hydrogenation of Carbon Dioxide to Methanol Catalyzed by Iron, Cobalt, and Manganese Cyclopentadienone Complexes: Mechanistic Insights and Computational Design. *Chem Eur J* **2017**, *23* (37), 8850–8856.

(53) Lu, X.; Zhang, Y.; Turner, N.; Zhang, M.; Li, T. Using Computational Methods to Explore Improvements to Knölker's Iron Catalyst. *Org Biomol Chem* **2014**, *12* (25), 4361–4371.

(54) Zhang, H.; Chen, D.; Zhang, Y.; Zhang, G.; Liu, J. On the Mechanism of Carbonyl Hydrogenation Catalyzed by Iron Catalyst. *Dalt Trans* **2010**, *39* (8), 1972–1978.

(55) Lu, X.; Zhang, Y.; Yun, P.; Zhang, M.; Li, T. The Mechanism for the Hydrogenation of Ketones Catalyzed by Knölker's Iron-Catalyst. *Org Biomol Chem* **2013**, *11* (32), 5264–5277.

(56) Lu, X.; Cheng, R.; Turner, N.; Liu, Q.; Zhang, M.; Sun, X. High Chemoselectivity of an Advanced Iron Catalyst for the Hydrogenation of Aldehydes with Isolated C=C Bond: A Computational Study. *J Org Chem* **2014**, *79* (19), 9355–9364.

(57) Ge, H.; Chen, X.; Yang, X. A Mechanistic Study and Computational Prediction of Iron, Cobalt and Manganese Cyclopentadienone Complexes for Hydrogenation of Carbon Dioxide. *Chem Commun* **2016**, *52* (84), 12422–12425.

(58) Zheng, Z.; Ma, X.; Cheng, X.; Zhao, K.; Gutman, K.; Li, T.; Zhang, L. Homogeneous Gold-Catalyzed Oxidation Reactions. *Chem Rev* **2021**, *121* (14), 8979–9038.

(59) Mato, M.; Franchino, A.; GarcÍa-Morales, C.; Echavarren, A. M. Gold-Catalyzed Synthesis of Small Rings. *Chem Rev* **2021**, *121* (14), 8613–8684.

(60) Li, Z.; Brouwer, C.; He, C. Gold-Catalyzed Organic Transformations. *Chem Rev* **2008**, *108* (8), 3239–3265.

(61) Corma, A.; Leyva-Pérez, A.; Sabater, M. J. Gold-Catalyzed Carbon-Heteroatom Bond-Forming Reactions. *Chem Rev* **2011**, *111* (3), 1657–1712.

(62) Arcadi, A. Alternative Synthetic Methods through New Developments in Catalysis by Gold. *Chem Rev* **2008**, *108* (8), 3266–3325.

(63) Hashmi, A. S. K. Gold-Catalyzed Organic Reactions. *Chem Rev* **2007**, *107* (7), 3180–3211.

(64) Jiménez-Núñez, E.; Echavarren, A. M. Gold-Catalyzed Cycloisomerizations of Enynes: A Mechanistic Perspective. *Chem Rev* **2008**, *108* (8), 3326–3350.

(65) Dorel, R.; Echavarren, A. M. Gold(I)-Catalyzed Activation of Alkynes for the Construction of Molecular Complexity. *Chem Rev* **2015**, *115* (17), 9028–9072.

(66) Asiri, A. M.; Hashmi, A. S. K. Gold-Catalysed Reactions of Diynes. *Chem Soc Rev* **2016**, *45* (16), 4471–4503.

(67) Campeau, D.; León Rayo, D. F.; Mansour, A.; Muratov, K.; Gagosz, F. Gold-Catalyzed Reactions of Specially Activated Alkynes, Allenes, and Alkenes. *Chem Rev* **2021**, *121* (14), 8756–8867.

(68) Cadierno, V. Gold-Catalyzed Addition of Carboxylic Acids to Alkynes and Allenes: Valuable Tools for Organic Synthesis. *Catalysts* **2020**, *10* (10), 1–37.

(69) Sankar, D. R.; Neetha, M.; Anilkumar, G. Gold-Catalyzed Lactone Synthesis: Advancements and Insights. *Chemical Record* **2024**, *24* (8), e202400071.

(70) Yoshikawa, K.; Takadera, T.; Adachi, K.; Nishijima, M.; Sano, H. Korormicin, a Novel Antibiotic Specifically Active against Marine Gram-Negative Bacteria, Produced by a Marine Bacterium. *J Antibiot* **1997**, *50* (11), 949–953.

(71) Babaei, G.; Aliarab, A.; Abroon, S.; Rasmi, Y.; Aziz, S. G. G. Application of Sesquiterpene Lactone: A New Promising Way for Cancer Therapy Based on Anticancer Activity. *Biomed Pharmacother* **2018**, *106*, 239–246.

(72) Paço, A.; Brás, T.; Santos, J. O.; Sampaio, P.; Gomes, A. C.; Duarte, M. F. Anti-Inflammatory and Immunoregulatory Action of Sesquiterpene Lactones. *Molecules* **2022**, *27* (3).

(73) Bińczak, J.; Dziuba, K.; Chrobok, A. Recent Developments in Lactone Monomers and Polymer Synthesis and Application. *Materials* **2021**, *14* (11).

(74) Schulz, S.; Hötling, S. The Use of the Lactone Motif in Chemical Communication. *Nat Prod Rep* **2015**, *32* (7), 1042–1066.

(75) Harkat, H.; Weibel, J. M.; Pale, P. A Mild Access to γ- or δ-Alkylidene Lactones through Gold Catalysis. *Tetrahedron Lett* **2006**, *47* (35), 6273–6276.

(76) Lin, B.; Yang, T.; Zhang, D.; Zhou, Y.; Wu, L.; Qiu, J.; Chen, G. Q.; Che, C. M.; Zhang, X. Gold-Catalyzed Desymmetric Lactonization of Alkynylmalonic Acids Enabled by Chiral Bifunctional P,N Ligands. *Angew Chem Int Ed* **2022**, *61* (23), e202201739.

(77) Sato, M.; Rawat, V. K.; Higashida, K.; Sawamura, M. Gold-Zinc Cooperative Catalysis for Seven-Exo-Dig Hydrocarboxylation of Internal Alkynes. *Chem Eur J* **2023**, *29* (56), e202301917.

(78) Peters, J.; Himo, F. Computational Study of Alkyne-Acid Cycloisomerization in Gold-Functionalized Resorcinarene Cavitand. *Chem Eur J* **2025**, e202404480.

(79) Goehry, C.; Besora, M.; Maseras, F. Computational Study on the Mechanism of the Acceleration of 1,3-Dipolar Cycloaddition inside Cucurbit[6]Uril. *ACS Catal* **2015**, *5* (4), 2445–2451.

(80) Rohling, R. Y.; Tranca, I. C.; Hensen, E. J. M.; Pidko, E. A. Mechanistic Insight into the [4 + 2] Diels-Alder Cycloaddition over First Row d-Block Cation-Exchanged Faujasites. *ACS Catal* **2019**, *9* (1), 376–391.

(81) Li, N.; Wang, Q.; Zhuo, S.; Xu, L. P. Mechanism and Origins of Selectivity in the Supramolecular [Ga4L6]12--Catalyzed Aza-Prins Reaction: The Mechanistic Studies. *ACS Catal* **2023**, *13* (16), 10531–10540.

(82) Xu, L.; Fang, G.; Tao, J.; Ye, Z.; Xu, S.; Li, Z. Molecular Mechanism and Solvation Effect of Supramolecular Catalysis in a Synthetic Cavitand Receptor with an Inwardly Directed Carboxylic Acid for Ring-Opening Cyclization of Epoxy Alcohols. *ACS Catal* **2018**, *8* (12), 11910–11925.

(83) Wang, K.; Jordan, J. H.; Hu, X. Y.; Wang, L. Supramolecular Strategies for Controlling Reactivity within Confined Nanospaces. *Angew Chem Int Ed* **2020**, *59* (33), 13712–13721.

(84) Gaeta, C.; La Manna, P.; De Rosa, M.; Soriente, A.; Talotta, C.; Neri, P. Supramolecular Catalysis with Self-Assembled Capsules and Cages: What Happens in Confined Spaces. *ChemCatChem* **2021**, *13* (7), 1638–1658.

(85) Leenders, S. H. A. M.; Gramage-Doria, R.; De Bruin, B.; Reek, J. N. H. Transition Metal Catalysis in Confined Spaces. *Chem Soc Rev* **2015**, *44* (2), 433–448.

(86) Endo, N.; Inoue, M.; Iwasawa, T. Rational Design of a Metallocatalytic Cavitand for Regioselective Hydration of Specific Alkynes. *Eur J Org Chem* **2018**, *2018* (9), 1136–1140.

(87) Schramm, M. P.; Kanaura, M.; Ito, K.; Ide, M.; Iwasawa, T. Introverted Phosphorus-Au Cavitands for Catalytic Use. *Eur J Org Chem* **2016**, *2016* (4), 813–820.

(88) Ho, T. D.; Schramm, M. P. Au-Cavitand Catalyzed Alkyne-Acid Cyclizations. *Eur J Org Chem* **2019**, *2019* (33), 5678–5684.

(89) Shi, Q.; Mower, M. P.; Blackmond, D. G.; Rebek, J. Water-Soluble Cavitands Promote Hydrolyses of Long-Chain Diesters. *PNAS* **2016**, *113* (33), 9199–9203.

(90) Wan, Y. H.; Zhu, Y. J.; Rebek, J.; Yu, Y. Recognition of Hydrophilic Cyclic Compounds by a Water-Soluble Cavitand. *Molecules* **2021**, *26* (7), 1922.

(91) Zhang, K. Da; Ajami, D.; Gavette, J. V.; Rebek, J. Alkyl Groups Fold to Fit within a Water-Soluble Cavitand. *J Am Chem Soc* **2014**, *136* (14), 5264–5266.

(92) Zhu, Y. J.; Zhao, M. K.; Rebek, J.; Yu, Y. Recent Advances in the Applications of Water-Soluble Resorcinarene-Based Deep Cavitands. *ChemistryOpen* **2022**, *11* (6), e202200026.

(93) Tang, M. M.; Kanagaraj, K.; Rebek, J.; Yu, Y. Role of Rim Functions in Recognition and Selectivity of Small-Molecule Guests in Water-Soluble Cavitand Hosts. *Chem Asian J* **2022**, *17* (15), e202200466.

(94) Castro-Puyana, M.; Marina, M. L.; Plaza, M. Water as Green Extraction Solvent: Principles and Reasons for Its Use. *Curr Opin Green Sustain Chem* **2017**, *5*, 31–36.

(95) Zhou, F.; Hearne, Z.; Li, C. J. Water—the Greenest Solvent Overall. *Curr Opin Green Sustain Chem* **2019**, *18*, 118–123.

(96) Ouyang, W. T.; Xiao, F.; Ou, L. J.; He, W. M. Green Photocatalytic Syntheses Using Water as Solvent/Hydrogen Source/Oxygen Source. *Curr Opin Green Sustain Chem* **2023**, *40*, 100760.

(97) Daver, H.; Harvey, J. N.; Rebek, J.; Himo, F. Quantum Chemical Modeling of Cycloaddition Reaction in a Self-Assembled Capsule. *J Am Chem Soc* **2017**, *139* (43), 15494–15503.

(98) Gaeta, C.; La Manna, P.; De Rosa, M.; Soriente, A.; Talotta, C.; Neri, P. Supramolecular Catalysis with Self-Assembled Capsules and Cages: What Happens in Confined Spaces. *ChemCatChem* **2021**, *13* (7), 1638–1658.

(99) Brea, O.; Daver, H.; Rebek, J.; Himo, F. Modeling Decomposition of N-Nitrosoamides in a Self-Assembled Capsule. *J Org Chem* **2019**, *84* (11), 7354–7361.

(100) Daver, H.; Rebek, J.; Himo, F. Modeling the Reaction of Carboxylic Acids and Isonitriles in a Self-Assembled Capsule. *Chem Eur J* **2020**, *26* (47), 10861–10870.

(101) Zhu, Y. J.; Zhao, M. K.; Rebek, J.; Yu, Y. Recent Advances in the Applications of Water-Soluble Resorcinarene-Based Deep Cavitands. *ChemistryOpen* **2022**, *11* (6), e202200026.

(102) Hutchins, J. B. Review: Acetylcholine as a Neurotransmitter in the Vertebrate Retina. *Exp. Eye. Res.* **1987**, *45* (1), 1–38.

(103) Wessler, I.; Kirkpatrick, C. J.; Racké, K. Non-Neuronal Acetylcholine, a Locally Acting Molecule, Widely Distributed in Biological Systems: Expression and Function in Humans. *Pharmacol Ther* **1998**, *77* (1), 59–79.

(104) Kihara, T.; Shimohama, S. Alzheimer's Disease and Acetylcholine Receptors. *Acta Neurobiol Exp* **2004**, *64* (1), 99–105.

(105) Szliszka, E.; Czuba, Z. P.; Domino, M.; Mazur, B.; Zydowicz, G.; Krol, W. Ethanolic Extract of Propolis (EEP) Enhances the Apoptosis- Inducing Potential of TRAIL in Cancer Cells. *Molecules* **2009**, *14* (2), 738–754.

(106) Wolfenden, R.; Yuan, Y. The "Neutral" Hydrolysis of Simple Carboxylic Esters in Water and the Rate Enhancements Produced by Acetylcholinesterase and Other Carboxylic Acid Esterases. *J Am Chem Soc* **2011**, *133* (35), 13821–13823.